SMALL ORGAN SIZE 1 and SMALL ORGAN SIZE 2/DWARF AND LOW TILLERING form a complex to integrate auxin and brassinosteroid signaling in rice

Authors:
Ko Hirano†*, Hideki Yoshida†, Koichiro Aya, Mayuko Kawamura, Makoto Hayashi, Tokunori Hobo, Kanna Sato-Izawa, Hidemi Kitano, Miyako Ueguchi-Tanaka*, and Makoto Matsuoka

Author affiliations:
Bioscience and Biotechnology Center, Nagoya University, Nagoya 464-8601, Japan.
†These authors contributed equally to this work.
*Corresponding authors. E-mail: khirano@nuagr1.agr.nagoya-u.ac.jp and muegu-chi@nuagr1.agr.nagoya-u.ac.jp
Tel: +81-52-789-5218

Running title:
Auxin and Brassinosteroid Crosstalk

Short Summary:
Auxin and brassinosteroid (BR) synergistically affect various physiological events, such as cell elongation and division, lateral root development, and promotion of rice lamina joint bending. An auxin regulated SMOS1 and a BR regulated SMOS2/DLT form a complex to integrate auxin and brassinosteroid signaling in rice.

Abstract

Although auxin and brassinosteroid (BR) synergistically control various plant responses, the underlying molecular mechanism of auxin-BR crosstalk is not well understood. We previously identified *SMOS1*, an auxin-regulated APETALA2-type transcription factor (TF), as the causal gene of the *small organ size 1* (*smos1*) mutant that is characterized by a decreased final size of various organs. In this study we identified another *smos* mutant, *smos2,* which shows a phenotype indistinguishable from *smos1*. *SMOS2* was identical to the previously reported *DWARF AND LOW-TILLERING (DLT)*, which encodes a GRAS protein involved in BR signaling. SMOS1 and SMOS2/DLT physically interact to cooperatively exhibit transactivation activity in yeast and in rice nuclei. Consistently, the expression of *OsPHI-1*, a direct target of SMOS1, is up-regulated only when SMOS1 and SMOS2/DLT proteins were both present in rice cells. These results suggest that SMOS1 and SMOS2/DLT form a keystone complex on auxin-BR signaling crosstalk in rice.

Keywords: auxin, brassinosteroid, crosstalk, rice, transcription factor.

Introduction

Phytohormones function coordinately in many aspects of plant growth and development, such as cell division and elongation, organ pattern formation, vegetative and reproductive development, and stress responses. There are five classical phytohormones, namely auxin, cytokinins, gibberellins (GAs), ethylene and abscisic acid (ABA), which were discovered by the mid-20th century. More recently, brassinosteroids (BRs), strigolactones, jasmonates and salicylic acid have also been defined as phytohormones. All of them have been linked to growth regulation either positively or negatively, and crosstalk between various phytohormone signaling pathways is now evident. Among them, there are extensive studies on crosstalk between auxin and BR signaling pathways, as they synergistically affect various physiological events, such as cell elongation and division, vascular differentiation, stimulation of ethylene biosynthesis, and tropism (Clouse and Sasse, 1998; Woodward and Bartel, 2005; Ibañes et al., 2009; Hardtke, 2007). For example, auxin and BR synergistically function to enhance hypocotyl elongation (Yopp et al., 1981; Katsumi, 1985; Nemhauser et al., 2004), and also lateral root development (Bao et al., 2004). They also promote the bending of the lamina joint of rice. The lamina joint is an organ between the leaf blade and leaf sheath, which acts as a hinge to bend the leaf

blade, and the degree of lamina inclination is determined by the cell elongation rate of the adaxial and abaxial cells of the lamina joint (Yokota and Mori, 1992). The lamina joint bending assay has been classically used as a bioassay to measure the level of BRs or auxin (Maeda, 1960; Maeda, 1961; Maeda, 1962; Maeda, 1965), and through this unique assay system, synergistic effects of auxin and BRs were elucidated (Mandava, 1988; Takeno and Pharis, 1982; Kim et al., 1990; Fujioka et al., 1998). Recently, it was demonstrated that BR inhibits the cell division at the abaxial side of the rice lamina joint (Sun et al., 2015).

The aforementioned synergetic effects of auxin and BRs on various physiological events have strongly suggested the interdependency of their signaling, and molecular evidence for this has been reported. For instance, the expression of early auxin-inducible genes, such as *indole-3-acetic acid* (*IAA*)*3*, *IAA5*, *SAUR-AC1*, and also DR5 promoter (a synthetic auxin responsive *cis*-acting element):GUS, is induced by exogenous brassinolide (BL) (Abel et al., 1995; Gil et al., 1994; Nakamura et al., 2003), whereas some of these genes are down-regulated in the BR-deficient mutant *de-etiolated2* (*det2*) (Nakamura et al., 2003). On the other hand, *DWARF4*, a gene encoding the rate determining step of BR biosynthesis, and also *BRASSINOSTEROID INSENSITIVE1* (*BRI1),* the BR receptor, are up-regulated by auxin (Nemhauser et al., 2004; Chung et al., 2011; Yoshimitsu et al., 2011; Sakamoto et al., 2012). Another example is that *BRASSINAZOLE RESISTANT 1* (*BZR1*), a transcription factor (TF) in the BR signaling pathway, can directly regulate multiple auxin-responsive genes (Sun et al., 2010). Furthermore, Nemhauser et al. (2004) found that one element highly over-represented in the promoters of genes induced by auxin and BR is responsive to both hormones, and that this element serves as a target for shared regulation by TFs downstream of each hormone. Goda et al. (2004) investigated the relationship between the actions of auxin and BR using a comprehensive expression profiling approach, and found that 48 genes are co-regulated by auxin and BL, including early auxin-responsive genes such as *SAUR, Aux/IAA* and *GH3*, whereas there are also many genes specifically regulated by either auxin or BL. They also found that a previously reported TGTCTC element in the auxin-responsive element (AuxRE) was not enriched in genes specifically regulated by auxin, but was enriched in genes up-regulated by both IAA and BL. These findings strongly suggest that the two hormone pathways affect gene expression in a coordinated manner at the transcriptional level.

We previously reported an unusual APETALA2 (AP2)-type TF carrying an imperfect AP2 domain, SMALL ORGAN SIZE1 (SMOS1), as the causal protein for a rice mutant having a decrease in the final size of various organs due to decreased cell size and abnormal microtubule orientation (Aya et al., 2014). *SMOS1* expression was induced by exogenous auxin treatment, and the AuxRE in the *SMOS1* promoter acts as a *cis*-regulatory element that interacts with AUXIN RESPONSIVE FACTOR (ARF) (Aya et al., 2014). We also identified rice *PHOSPHATE-INDUCED PROTEIN-1 (OsPHI-1),* which is involved in cell expansion, as a target gene of SMOS1 by gel-shift and chromatin immunoprecipitation (ChIP) experiments (Aya et al., 2014). Down-regulation of *OsPHI-1* in rice leads to reduced plant height, thickened culm, reduced cell size and increased cell number, and aberrant microtubule orientation, which all resembles to that of *smos1*, suggesting that down regulation of *OsPHI-1* in *smos1* is, at least in part, responsible for the *smos1* mutant phenotype (Aya et al., 2014). Since *SMOS1* homologs of lycophyta (*Selaginella moellendorffii*) and moss (*Physcomitrella patens*) can complement the rice *smos1* mutant when over-expressed, it suggests that *SMOS1* is widely conserved in the plant kingdom (Aya et al., 2014). In the current report, we identified a SMOS1-interacting protein, SMOS2, through positional cloning of the causal gene of another *small organ size* mutant, *smos2,* a mutant showing phenotype indistinguishable from *smos1*. *SMOS2* encodes a GRAS protein, which was previously reported as a protein involved in BR signaling, DWARF AND LOW-TILLERING (DLT) (Tong et al., 2009). Both SMOS1, under the control of auxin signaling, and SMOS2/DLT, under the control of BR signaling, are essential for the expression of *OsPHI-1,* indicating that the interaction between these SMOS proteins is a crosstalk point for auxin and BR signaling.

Results

A new *smos* mutant, *smos2,* is related to the *smos1* mutant. A rice mutant, *smos1*, shows semi-dwarf and erect-leaf phenotypes with small size of various organs such as leaf, root, stamen, pistil, and seed (Figure 1A and Aya et al., 2014). During *smos1* screening, we identified several additional mutants with phenotypes similar to that of *smos1*, but not allelic to *smos1*. Among them, we focused on two *smos* mutants and named them *smos2-1* and *smos2-2*. *smos2* showed semi-dwarf height (Figure 1A, B and Supplementary Table 1), shortened cell length, and aberrant cell arrangement in the root and leaf sheath, similar to *smos1* (Supplementary Figure 1). To analyze the relationship between *SMOS1* and *SMOS2*, we produced a double

mutant by crossing the *smos1-3* and *smos2-2* mutants, which were derived from the same background, Nipponbare, and compared this double mutant with *smos1* and *smos2*. The phenotype of the double mutant was indistinguishable from *smos1* and *smos2* in terms of dwarfism, increased culm width, and increased cell number (Figure 1A-E).

Since these morphological observations suggest that *smos1* and *smos2* are related, we further examined the relationship between *SMOS1* and *SMOS2* in terms of molecular biological function and compared the gene expression patterns of the *smos1* and *smos2* mutants (Figure 1F). Among the 1695 genes differentially expressed in the developing culm internodes between *smos1* and WT at a significant level ($p < 0.001$, FDR < 0.01, ≥ 2-fold difference) (Supplementary Table 2), most of them were regulated in a similar manner in *smos2*, with a high correlation coefficient (R^2=0.8173), and 74.9% of the genes differentially expressed between *smos1* and WT were also differentially expressed in *smos2*. However, the regression line was calculated as y=0.7232x – 0.0377, indicating that there are also differences between *smos1* and *smos2*. Furthermore, some probes were arranged around the y=0 line, indicating that the expression of these probes was changed only in *smos1,* and not in *smos2*. These observations strongly suggest that *SMOS1* and *SMOS2* are involved in a similar gene expression mechanism with slight differences.

Map-based cloning of *SMOS2*. To identify the *SMOS2* locus, we performed map-based cloning. By crossing *smos2-1* with an *indica* variety, Kasalath, the *SMOS2* locus was mapped on the short arm of chromosome 6 between molecular markers D38 and RM276 (Figure 2A top panel). In a subsequent screen of 2,000 F2 plants, *SMOS2* was localized to a 22.6-kb region mapped between markers SNP038 and RM586, which contained 7 genes. By sequencing this region, we detected a 510-bp deletion, which included the translation start site of a transcript (AK106449) of Os06g03710 that encodes a GRAS protein previously named OsGRAS32 (Tian et al., 2004). As expected, the genomic sequence of Os06g03710 in *smos2-2* also contained a one-nucleotide insertion in its coding region (Figure 2B). To confirm that the *smos2* mutations are caused by loss-of-function of Os06g03710, we introduced the entire genomic region encompassing the 5'- and 3'-flanking sequences into *smos2-1* and *smos2-2*. The semi-dwarf and erect-leaf phenotypes of *smos2* were rescued by its introduction (Figure 2C and Supplementary Figure 2), demonstrating that Os06g03710 is the causal gene for *smos2*. A

loss-of-function mutant of Os06g03710 has been previously reported as *dwarf and low-tillering, dlt*, which shows a similar phenotype to *smos2* (Tong et al., 2009). We refer to Os06g03710 as *SMOS2*/*DLT* hereafter.

Cooperative function of SMOS1 and SMOS2/DLT. To examine how *SMOS1* and *SMOS2*/*DLT* function cooperatively, we first examined their expression in various organs in the Rice Expression Profile Database (http://ricexpro.dna.affrc.go.jp/), and found that the expression pattern of these genes is relatively similar (Supplementary Figure 3). Next, we performed yeast two-hybrid assays (Y2H) to test the physical interaction between SMOS1 and SMOS2/DLT. As expected, these proteins tightly bind in yeast (Figure 3A). To precisely investigate the SMOS1 and SMOS2/DLT interaction, we physicochemically analyzed this interaction using surface plasmon resonance (SPR) (Figure 3B). In this experiment, the k_a (association) value for the SMOS1-SMOS2/DLT interaction was estimated as 1.2 X 10^5 (M^{-1} s^{-1}) and the k_d (dissociation) value was 1.8 X 10^{-3} (s^{-1}); consequently, the *K*D (affinity) was calculated as 1.5 X 10^{-8} (M) (Supplementary Table 3). SMOS1-SMOS2 interaction was also confirmed in rice mesophyll protoplasts by co-immunoprecipitation assay (Figure 3C).

As *SMOS1* and *SMOS2*/*DLT* encode AP2 and GRAS proteins, respectively, both of which have been considered to be involved in transcriptional regulation, we directly examined their transactivation activity by fusing them with the GAL4 DNA-binding domain (GAL4DB) without a prey construct (Figure 3D). These fusion proteins alone did not activate transcription of the target gene, *β-galactosidase* (β-Gal), indicating that these proteins do not contain intrinsic transactivation activity in yeast cells. However, when GAL4DB-SMOS1 was co-expressed with SMOS2/DLT, a significant level of β-Gal activity was detected, and vice versa (Figure 3D). These findings suggest that SMOS1 and SMOS2/DLT interact and the complex possesses transactivation activity, though each protein alone hardly does.

SMOS1 and SMOS2/DLT cooperatively function to enhance the transcription of a SMOS1-target, *OsPHI-1*, in rice cells. The above observations suggest that SMOS1 and SMOS2/DLT cooperatively function to enhance the expression of their target genes. As SMOS1 contains the AP2 DNA binding domain (DBD), whereas SMOS2/DLT is a GRAS protein assumed to function as transcriptional co-regulator (Sun et al., 2012), we predicted

that SMOS1 functions as the DNA-binding component of the transactivation complex. To examine this possibility, we first generated transgenic plants over-expressing *SMOS1* fused with a SRDX motif, a motif which suppresses the transactivation activity of the fused protein (Oshima et al., 2011). Plants overexpressing SMOS1-SRDX mimicked the phenotype of *smos1,* including semi-dwarfism, abnormal cell arrangement of the leaf sheath, and enhanced culm width with increased cell number (Figure 4A-C). Next, we over-expressed the *SMOS1* cDNA under the control of the *Actin* promoter (*pActin*) in *smos1* and *smos1/smos2 (dlt)* mutants. Over-expression of *SMOS1* rescued the dwarf phenotype and decreased the culm width and cell number of the *smos1* mutant, but not of *smos1/smos2(dlt)* (Figure 4D,E). Previously, we reported the aberrant microtubule organization and abnormal cell division in the stem and leaf sheath cells of *smos1*, and suggested that this is the cause of dwarfism, decreased cell size, and abnormal cell arrangement (Aya et al., 2014). Such aberrant microtubule organization was observed in the leaf sheath cells of both *smos2* and *smos1/smos2(dlt)* mutants (Figure 4F). Over-expression of *SMOS1* rescued the disorganization of *smos1*, but not of the *smos1/smos2(dlt)* double mutant, suggesting that SMOS2/DLT is required for SMOS1 to activate transcription in rice.

Our previous experiments revealed that such aberrant microtubule organization of stem and leaf sheath cells depends, at least in part, on the down regulation of the SMOS1 target gene, *OsPHI-1* (Aya et al., 2014). This was also supported by the fact that the OsPHI-1 homolog in *Arabidopsis* functions as a positive regulator for cell expansion (Schröder et al., 2009). Thus, we examined the expression of *OsPHI-1* in *smos2* and *smos1/smos2(dlt)* mutants (Figure 5). The expression of *OsPHI-1* decreased in *smos1*, as previously reported (Aya et al., 2014), and also in the *smos2(dlt)* and *smos1/smos2(dlt)* mutants (Figure 5A), indicating that *OsPHI-1* is a target gene of the transcriptional complex of SMOS1 and SMOS2/DLT. To confirm this, we examined *OsPHI-1* expression in *smos1* and *smos1/smos2(dlt)* mutants over-expressing *SMOS1* (Figure 5B). Its expression was dramatically enhanced in the *SMOS1* over-expressing *smos1* mutant, but not in the double mutant. We also examined the transient expression of *OsPHI-1* in *smos1/smos2* double mutant callus cells, which were bombarded with *pActin::SMOS1* and/or *pActin::SMOS2/DLT* as effectors and *pOsPHI-1::rennila Luciferase* (*rLUC*) as a reporter (Figure 5C). Bombardment of *SMOS1* or *SMOS2*/*DLT* alone did not or only slightly enhanced the *rLUC* expression, respectively, but co-bombardment of both effec-

tors doubled the transcription compared to the vector control. This interdependent transcriptional activity indicates that the SMOS1-SMOS2 complex acts as a transactivating complex on the *OsPHI-1* promoter to regulate plant organ size. The slight but significant up-regulation of transactivation activity observed in SMOS2/DLT-bombarded callus compared to the vector control (Fig 5C) suggests that apart from SMSO1, SMOS2/DLT might also interact with another factor in rice.

The SMOS1-SMOS2/DLT interaction occurs via the C-terminal conserved motif of SMOS1. Our previous study revealed that SMOS1 contains four unique conserved motifs outside of the AP2 domain; AKER, EPY, ILS, and WTNF (named after their most conserved amino acids), which are shared with the SMOS1 homologs in pine, *Selaginella moellendorffii* and *Physcomitrella patens* (Figure 6A) (Aya et al., 2014). We suspected that these conserved motifs are involved in the SMOS1-SMOS2/DLT interaction, and produced a series of internal deletions for each motif of SMOS1, and tested its interaction with SMOS2/DLT by Y2H (Figure 6B). Deletion of each motif except for the WTNF motif did not affect the SMOS1-SMOS2 interaction; however, deletion of the WTNF motif located at the very C-terminal side dramatically diminished the SMOS1-SMOS2/DLT interaction. We also performed a transient assay of *pOsPHI-1::rLUC* expression in the cells of the double mutant using the same internal deletion series of SMOS1 as above, and confirmed that deletion of the WTNF motif diminishes the transactivation activity of SMOS1 even in the presence of SMOS2/DLT (Figure 6C), suggesting that WTNF motif interacts with SMOS2/DLT. Next, we examined the effect of the WTNF motif on the SMOS1-SMOS2/DLT interaction by a split-YFP (yellow fluorescent protein) system (Figure 6D). We fused SMOS1 with the C-terminal fragment of enhanced yellow fluorescent protein (cEYFP) and SMOS2/DLT with its N-terminal fragment (nEYFP), and introduced these plasmids into rice protoplast cells. Fluorescent signal was observed in the nucleus by co-introduction of the intact SMOS1-cEYFP and SMOS2/DLT-nEYFP, while co-introduction of (ΔWTNF) SMOS1-cEYFP and SMOS2/DLT-nEYFP did not cause any signal. Furthermore, we confirmed the effect of the WTNF motif deletion on SMOS1-SMOS2/DLT function *in planta* (Figures 6E, F), and found that its deletion failed to rescue the abnormal phenotypes of *smos1*. All of these results demonstrate that SMOS1 and SMOS2/DLT interact via the WTNF motif of SMOS1 and collaboratively function as a transactivation complex in nuclei.

Interaction of SMOS1 and SMOS2/DLT is a crosstalk point for auxin and BR signaling. Previously, Tong et al. (2012) reported that SMOS2/DLT is a positive regulator of BR signaling, and its function is negatively regulated by BRASSINOSTEROID INSENSITIVE 2 (BIN2); whereas we reported that *SMOS1* expression is regulated by auxin signaling, and its expression is positively regulated by OsARF1 (Aya et al., 2014) (Figure 7A). These observations suggest that the interaction between SMOS1 and SMOS2/DLT might be a crosstalk point for auxin and BR signaling. To confirm this hypothesis, we examined the expression of *OsPHI-1* (Figure 7B), and found that its expression was extensively enhanced by application of BL in rice WT seedlings, whereas BL treatment did not enhance *SMOS1* expression (Figure 7C), nor *OsPHI-1* expression in *smos1* or *smos2* mutants (Figure 7B). These results indicate that the *OsPHI-1* expression is positively regulated by BR collaborating with SMOS1, but SMOS1 expression does not depend on BR. Next, we studied the dependency of the *OsPHI-1* expression on auxin signaling. First, we examined the effect of indole acetic acid (IAA) on *OsPHI-1* expression. We treated plants with IAA and measured the *OsPHI-1* expression at various time points, which demonstrated that the gene expression substantially increased at 1 hr of treatment (Figure 7D). Expression of *OsIAA3,* a gene known to be positively regulated by auxin, was also confirmed to be up-regulated by IAA treatment (Supplementary Figure 4A). When plants were treated with *p*-phenoxyphenyl boronic acid (PPBo), an inhibitor of an auxin biosynthesis enzyme, YUCCA (Kakei et al., 2015), as expected, dramatically diminished the expression of *OsIAA3* (Supplementary Figure 4B), and also *SMOS1* and *OsPHI-1* (Figure 7E-F), while expression of *SMOS2*/*DLT* was unaffected (Figure 7G). We also over-expressed the constitutive active form of *IAA3 (IAA3 P58L)* in rice (Inukai et al., 2005), and analyzed the expression of *OsPHI-1*, *SMOS1*, and *SMOS2*. Although it was not significant, expression of *SMOS1* had a tendency to decrease, and *OsPHI-1* expression significantly decreased in *IAA3 P58L* introduced rice compared to the WT, whereas expression of *SMOS2* was unaltered (Figures 7H-J). The above observations support that *OsPHI-1* is positively controlled by auxin via SMOS1 function.

Next, to gain insight on how common SMOS1-SMOS2 complex account for auxin-BR crosstalk observed in rice, we analyzed the lamina joint bending of *smos* mutants, since lamina joint is regulated by auxin and BR (Mandava, 1988; Takeno and Pharis, 1982; Kim et al., 1990; Fujioka et al., 1998). In WT, auxin slightly and BR significantly enhanced, whereas

simultaneous application of both hormones synergistically enhanced the bending (Figure 7K). When *smos* mutants were treated with auxin and/or BL, they all showed attenuated bending compared to those of WT, suggesting that the SMOS1-SMOS2/DLT complex might also act as a crosstalk point of auxin-BR signaling on lamina joint bending in rice.

SMOS1 interacts with various rice GRAS proteins. GRAS proteins are thought to function as transcriptional co-regulators assumed to lack the ability to bind to DNA (Tian et al., 2004), and are known to interact with various TFs through their GRAS domains (Yoshida et al., 2014). We hypothesized that SMOS1 might also interact with other GRAS proteins in addition to SMOS2/DLT and investigated SMOS1-GRAS protein interaction by Y2H. 8 out of 17 GRAS proteins interacted with SMOS1, including the rice DELLA protein, SLR1 (Supplementary Figure 5), indicating that SMOS1 might form complexes with other GRAS protein to exhibit various biological functions.

Discussion

At present, the molecular mechanism of auxin and BR signaling has been clarified as follows. Upon perception of auxin by TRANSPORT INHIBITOR RESPONSE 1 (TIR1) receptor, TIR1 gains a higher interaction affinity for transcriptional repressors, Aux/IAA proteins, resulting in Aux/IAA degradation. Aux/IAAs inhibit the function of ARFs, positive transcriptional regulators of auxin inducible genes. Thus, Aux/IAA degradation results in the activation of auxin inducible gene expression (Figure 7A) (Wright and Nemhauser, 2015). In the case of BR signaling, BR is perceived by BRI1 receptor kinase. BIN2, a cytoplasmic Ser/Thr kinase, is a negative regulator of BR responses and in the absence of BR, BIN2 constitutively phosphorylates transcriptional regulators involved in BR response, such as BZR1 and BRI1-EMS suppressor 1 (BES1) to block further transduction of BR signaling. Activation of BRI1 by BR perception inhibits the function of BIN2, resulting in BZR1- and BES1-mediated expression of various BR-induced genes (Zhu et al., 2013).

As mentioned in the introduction, many transcriptional target genes are shared by auxin and BR (Nemhauser et al., 2004; Goda et al., 2004; Goda et al., 2002; Müssig et al., 2002; Yin et al., 2002; Nemhauser et al., 2006), suggesting that interactions between TFs involved in auxin and BR act as a point of auxin-BR crosstalk but only a few such cases have been reported. One is the response of *SAUR15* to auxin and BR. *SAUR15* expression depends on the

simultaneous interaction of BES1 and MONOPTEROS (MP)/ARF5 within the *SAUR 15* promoter, a Hormone Up at Dawn (HUD)-type E-box and AuxRE cis elements, respectively (Walcher and Nemhauser, 2012). Another example is that BZR1 and ARF6 were shown to interact and regulate a large number of common target genes (Oh et al., 2014).

In the current study, we showed a novel type of crosstalk between auxin and BR signaling, which occurs through the interaction of SMOS1 and SMOS2/DLT (Figure 7A). Regulation of *SMOS1* expression by auxin signaling was previously reported by Aya et al. (2014), and confirmed in this study using an auxin synthesis inhibitor, PPBo and by over-expressing IAA3 (P58L) in rice (Figure 7E and H). Interestingly, auxin continuously induced *SMOS1* (Aya et al., 2014) but induction of *OsPHI-1* by auxin was observed only at 1 h after auxin treatment (Fig. 7D). Possibly, rapid feedback regulation of *OsPHI-1* expression by an unknown factor has occurred. In contrast, SMOS2/DLT is a member of the GRAS family of transcriptional co-regulators and plays a positive role in BR signaling in rice (Tong et al., 2009). Tong et al. (2012) further demonstrated that rice BIN2 kinase directly interacts with SMOS2/DLT to phosphorylate it, whereas BL induces the dephosphorylation of SMOS2/DLT. Based on this observation, they suggest that SMOS2/DLT is a substrate of BIN2.

Interestingly, *smos1* and *smos2* mutants both show increased cell number. This may seem counterintuitive because auxin and BR can promote cell proliferation (Wright and Nemhauser, 2015; Perrot-Rechenmann, 2010). However, in some contexts the two hormones inhibit cell proliferation, such as at a high concentration and in abaxial cells of rice lamina joint (Hardtke, 2007; Sun et al., 2015). Given these knowledge, the increased cell numbers of *smos* mutants seem to result from complex integration of auxin and BR signaling.

Our observations in this study demonstrated that physical interaction of SMOS1 and SMOS2/DLT positively regulates the expression of *OsPHI-1*. Indeed, the loss-of-function mutants of *SMOS1* or *SMOS2*/*DLT* showed similar phenotypes in terms of their morphologies, such as semi-dwarfism, enlarged culm thickness, abnormal cell arrangement and increased cell number (Figure 1A-E and Supplementary Figure 1), and also similar expression profiles (Figure 1F). Their physical interaction effectuates the transactivation activity, while each protein alone is incapable or only slightly activates the transcription of an actual target in rice cells, *OsPHI-1* (Figure 5). Consequently, the interaction between SMOS1 and SMOS2/DLT, which are under the control of auxin and BR signaling, respectively, is an actual crosstalk point for these signaling pathways (Figure 7A). The fact that *smos1* and *smos2*

both show attenuated lamina joint bending also supports the idea that SMOS1-SMOS2 complex functions in auxin-BR crosstalk.

Since the early discovery of the auxin-BR crosstalk on lamina joint bending (Maeda, 1965), several papers addressing the causal genes of the crosstalk have been published (Luo et al., 2016). For example, a recent paper demonstrated that a transcription factor, LPA1, negatively regulates lamina joint bending by inhibiting BR signaling and by increasing the expression of auxin transporters (Liu et al., 2016). In the current study, we revealed the molecular mechanism, which underlies the auxin-BR crosstalk in rice. Because treatment of auxin and BR to *smos* mutants still shows a synergistic effect on lamina joint bending (Fig. 7K), it is plausible that lamina joint bending is determined by a transcriptional network consisting of SMOSs, LPA1 and possibly other factors regulated by auxin and BR signaling.

The molecular concept of such crosstalk, consisting of a DNA-binding TF (SMOS1) and co-regulator (SMOS2/DLT), is a common phenomenon observed in animal and yeast cells. Actually, some TFs carrying DNA-binding domains interact with over one thousand kinds of co-regulators to form various complexes (Millard et al., 2013). Such a regulatory mechanism is thought to provide significant benefits to organisms, because environmental signals can be rapidly transmitted through changing the interacting co-regulators. In plants, only a few cases of signaling crosstalk via TFs and co-regulators has been reported, for example, ABI3 and ABI5, positive TFs of ABA signaling, interact with DELLA proteins, negative regulators of GA signaling, to enhance transcription of *SOMNUS*, a repressor of germination (Lim et al., 2013). In the current study, Y2H revealed that SMOS1 carrying the AP2 DNA-binding domain interacts not only with SMOS2/DLT, but also with other GRAS proteins (Supplementary Figure 5). Since many GRAS possess transactivation activity (Sun et al., 2012), it is suggested that a mechanism may exist in which SMOS1 switches its interacting GRAS partner in response to multiple environmental signals, as in animal and yeast cells. Furthermore, the fact that the co-regulator activity of SMOS2/DLT is regulated in a phosphorylation-dependent manner by the BIN2 kinase (Tong et al., 2012) is homologous to animals. Indeed, a human co-regulator, SMRT, is phosphorylated by a protein kinase and released from the nuclear receptor to relocate in the cell (Varlakhanova et al., 2011). In conclusion, our present findings reveal the crosstalk point of the auxin and BR signaling pathways via SMOS1 and SMOS2/DLT, and emphasize the similarity of transcriptional regulation mechanism between

animal and plant to implement signaling crosstalk.

Methods

Plant materials and growth conditions. The *smos1-1* mutant was identified from a mutant library of *Oryza sativa* cv. Taichung 65 mutagenized with *N*-methyl-*N*-nitrosourea (MNU). *smos1-3* and *smos2-2* were obtained from a public *TOS17* mutant library of *O. sativa* cv. Nipponbare (http://tos.nias.affrc.go.jp/~miyao/pub/tos17/index.html). *smos2-1* was generated from gamma ray irradiated Nipponbare. The *smos1-3/smos2-2* double mutant was generated by crossing *smos1-3* and *smos2-2* using the latter as the pollen donor.
Rice plants were cultivated under greenhouse conditions (15 h light, 25^{o}C) and subsequently transplanted to paddy fields until they reached the heading stage.

Confirmation of the *smos1-3*/*smos2-2* mutation by PCR. The *SMOS1* and *SMOS2*/*DLT* genes in the *smos1-3*/*smos2-2* mutant were amplified by PCR using gene-specific primers. Mutations were confirmed by sequencing the PCR fragment for *SMOS1* and by restriction digestion for *SMOS2*/*DLT*. Primer sequences are listed in Supplementary Table 4.

Rice used for expression analysis. Seedlings of WT, mutants, and transgenic rice were grown for 10 days in the greenhouse, and seedlings were cut approximately 1 cm from the base and collected to analyze *OsPHI-1* expression.

To examine the expression of *SMOS1*, *SMOS2*/*DLT* and *OsPHI-1* after exogenous auxin (IAA), auxin inhibitor PPBo (p-phenoxyphenyl boronic acid) and brassinolide (BL) treatment, seeds were sterilized in 1% NaClO for 20 min and sown on Murashige and Skoog (MS) agar medium. The seedlings were grown in a growth chamber at 30°C under continuous light. For IAA treatment, 10-day-old seedlings were transferred into containers filled with water after removing the agar medium form the roots, and grown for another 2 days. After acclimatization, seedlings were submerged for 2 h in a solution of 10 μM IAA or 0.1% ethanol (mock treatment), and RNA was extracted from seedlings cut approximately 1 cm from the base. For PPBo and BL treatment, seedlings were grown in either MS agar containing 1 μM BL (Daiichi Fine Chemical) dissolved in ethanol or 40 μM PPBo dissolved in DMSO, and RNA was extracted from 10-day-old seedlings. Mock-treated plants were grown either in MS agar containing 0.01 % ethanol or 0.01 mM DMSO, respectively.

Plasmid construction. PCR amplification for all constructs was performed using high-fidelity PrimeStar DNA polymerase (Takara). Primer sequences are listed in Supplementary Table 4. PCR-amplified fragments were sequenced to ensure that no mutations were introduced.

For the transient expression analysis, *SMOS1* and *SMOS2*/*DLT* were each cloned into the *Xba*I/*Sma*I site of *pACT/pUC19* to produce *pACT-SMOS1/pUC19* and *pACT-SMOS2/pUC19*, respectively. The *OsPHI-1* promoter region (2.0 kb upstream from the *OsPHI-1* start codon) was cloned into the *Sal*I/*Sma*I site of *Renilla LUC (rLUC)/pUC19* to produce *pOsPHI-1-rLUC/pUC19*. To introduce the *SMOS1* internal deletion series into *pACT/pUC19*, *SMOS1* was first cloned into a TOPO vector (Invitrogen). Next, PCR was performed to amplify the entire plasmid except for the motif to be deleted. After phosphorylation of the PCR fragment, the parental methylated and hemimethylated DNA in the PCR reaction mixture was digested with *Dpn*I, and the deletion-containing *SMOS1/TOPO* vector was self-ligated and transformed into *E. coli* XL10-Gold (Stratagene) to produce *SMOS1* with an internal deletion in the TOPO vector. Lastly, the plasmid was PCR-amplified and cloned into the *Xba*I/*Sma*I site of *pACT/pUC19*.

To produce the *SMOS2*/*DLT* complementation construct, a 6.5-kb genomic DNA fragment containing the full-length rice *SMOS2*/*DLT* gene was PCR-amplified using Nipponbare genomic DNA as a template. This fragment was then subcloned into the *Sma*I site of the *pBI Hm 12* binary vector (Ohta et al., 1990) to generate the *SMOS2*/*DLT* complementation construct.

To produce BD-SMOS1 and AD-SMOS2/DLT for Y2H analysis, *SMOS1* and *SMOS2*/*DLT* were PCR-amplified using Nipponbare cDNA, and cloned into the *Eco*RI/*Sma*I site of *pBridge* and the *Eco*RI/*BamH*I site of *pGADT7*, respectively. To produce a plasmid that co-express BD-SMOS1 and SMOS2/DLT in yeast, *SMOS2*/*DLT* was cloned into the *Not*I/*Bgl*II site of *BD-SMOS1/pBridge*. Similarly, *SMOS1* was cloned into the *Not*I/*Bgl*II site of *BD-SMOS2/pBridge* to co-express BD-SMOS2 and SMOS1 in yeast. To construct the *SMOS1* internal deletion series fused with *AD*, each *SMOS1* internal deletion sequence cloned into the TOPO vector was PCR-amplified and cloned into the *Eco*RI/*Sma*I site of *pGADT7* to produce SMOS1 proteins containing internal deletions fused with the AD. GRAS members other than *SMOS2*/*DLT*, including *OsGRAS1-15* and *OsGRAS20* (*Os01g67650, Os02g10360, Os05g31380, Os05g42130, Os06g01620, Os07g38030, Os07g39820,*

Os07g40020, Os03g31880, Os11g47890, Os11g47900, Os11g47920, Os12g04380, Os02g45760, Os03g15680, Os05g49930), were also PCR-amplified using Nipponbare cDNA, and cloned into the *Eco*RI/*Sma*I (*OsGRAS1-13*) or *Eco*RI/*Cla*I (*OsGRAS14, 15, 20*) site of *pGADT7*.

For the surface plasmon resonance experiment, *SMOS1* was first cloned into the *Eco*RI/*Sal*I site of *pGBKT7* to produce *cMYC-SMOS1*. Next, *cMYC-SMOS1* was cloned into the *BamH*I/*Xho*I site of *pGEX6p-1* to express GST-cMYC-SMOS1. To produce MBP-3xFLAG-SMOS2/DLT, *SMOS2*/*DLT* was first cloned into the *Sma*I/*Spe*I site of *pACT-3xFLAG/pCAMBIA* (Hirano et al., 2010), and subsequently, *3xFLAG-SMOS2/DLT* was cloned into the *BamH*I/*Eco*RI site of *pMAL-c5x*.

For the transgenic experiment, the maize ubiquitin promoter and the omega sequence were simultaneously cloned into the *Eco*RI/*Sma*I site of *pCAMBIA1380* to produce *pUbi-omega/pCAMBIA*. Next, *SMOS1* was cloned into the *BamH*I/*Spe*I site of *pUbi-omega/pCAMBIA* to produce *pUbi-omega-SMOS1/pCAMBIA* to over-express *SMOS1* in rice. For the SRDX experiment, *SMOS1* was cloned into the *Xba*I/*Sma*I site of *pACT-SRDX/pCAMBIA* (Hirano et al., 2013) to produce *pACT-SMOS1-SRDX/pCAMBIA*. To over-express ΔWTNF-SMOS1 in rice, *ΔWTNF-SMOS1* was PCR-amplified using *SMOS1* as the DNA template and cloned into the *BamH*I/*Spe*I site of *pACT/pCAMBI*A. To produce rice overexpressing *OsIAA3 (P58L)*, *OsIAA3* was PCR-amplified with primers SmaI+IAA3.F and IAA3.R+SmaI using Nipponbare cDNA and cloned into TOPO-blunt (Invitrogen). Next, to introduce C173T mutation into *OsIAA3*, which results in proline to leucine amino acid change, primers containing C173T mutation were PCR-amplified with either SmaI+IAA3.F or IAA3.R+SmaI to generate two partially overlapping partial IAA3 (C173T) DNA. Subsequently these two DNA were mixed and used as a template to PCR-amplify the full-length IAA3 (C173T) coding sequence. Amplified DNA was cloned into the *Sma*I site of *pUbi-omega/pCAMBIA* to produce *pUbi-omega-OsIAA3 (P58L)/pCAMBIA*.

To produce SMOS1-cEYFP and SMOS2/DLT-nYFP for the BiFC experiment, *SMOS1* and *SMOS2*/*DLT* were introduced into *TOPO-D/pENTR* (Invitrogen) to generate the entry clones. The *SMOS1* and *SMOS2*/*DLT* constructs were used to clone the CDS into the vectors *pGWcY* and *pGWnY* by the LR Gateway reaction to generate C- and N-terminal fusions to the two YFP fragments (Hino et al., 2011).

For the co-immunoprecipitation experiment, the coding sequences of HA was generated by annealing two oligo-nucleotides (F_HAtag infusionOligo and R_HAtag infusionOligo, see Supplementary Table 4) following the manufacturer's instructions (Sigma-Aldrich). The coding sequence of *3 x FLAG* was amplified by PCR. These HA and FLAG sequences were inserted into the *Stu*I-*Spe*I site of *pE2113_GW_SAS* (Yoshida et al., 2014) to generate *pE2113_GW_HA* and *pE2113_GW_FLAG* vectors, respectively. The coding sequence of *SMOS1* was PCR-amplified and cloned into *Xba*I-*Spe*I site of *pE2113_GW_HA* by NEBuilder HiFi DNA Assembly master mix (New England BioLabs). The entry clone containing *SMOS2/DLT* was used to clone *SMOS2* into *pE2113_GW_FLAG* by LR Gateway reaction (Invitrogen).

Yeast Two-Hybrid The yeast two-hybrid assay (Y2H) was performed as described previously (Ueguchi-Tanaka et al., 2005) using the BD Matchmaker Two-Hybrid System 3 (Clontech). Vector cassettes for DNA-BD and -AD (activation domain) were used as negative controls, and *Saccharomyces cerevisiae* strain Y187 was used as the host. Experiments were independently repeated at least three times. Details of the methods used for the yeast assays can be found in the manufacturer's instructions (Yeast Protocols Handbook #PT3024-1; http://www.clontech.com/).

Affinity and Kinetic Studies. To produce recombinant GST-cMYC-SMOS1 and MBP-3xFLAG-SMOS2/DLT in *E. coli*, the BL21 (DE3) pLysS Rosetta-gami2 (Novagen) strain harboring the *pGEX GST-cMYC-SMOS1* vector and the *pMAL-c5x MBP-SMOS2/DLT* vector was first incubated at 37°C until reaching an OD600 of 0.4 to 0.6. The *E. coli* was then incubated at 18°C, 0.2 mM isopropyl-b-D-thiogalactopyranoside (IPTG) was added, and the *E. coli* was incubated for an additional 18 h. For the purification of GST-cMYC-SMOS1, cells were harvested and resuspended with buffer A (20 mM Tris-HCl, pH 7.5, 200 mM NaCl, 1 mM DTT, and 15 mM n-octylglucoside) and lysed by sonication (20 kHz, 5 sec X 40 times). The lysate was centrifuged at 16,000g for 30 min, and the supernatant was mixed with Glutathione Sepharose 4B (GE Healthcare) equilibrated with buffer B (200 mM NaCl, 20 mM Tris-HCl pH 7.5, 1 mM DTT, and 10 mM n-octylglucoside) and rotated for 1 h at 4°C. The resin was washed five times with buffer B and eluted five times with 400 μL of 20 mM glutathione in buffer B.

For the purification of MBP-SMOS2/DLT, cells were harvested and resuspended with buffer C (20 mM Tris-HCl, pH 7.5, 200 mM NaCl, 1 mM DTT, and 1 mM EDTA) and lysed and centrifuged as described above. The supernatant was mixed with Amyrose Resin (BioLabs) and rotated for 1 h at 4°C. The resin was washed five times with buffer C and eluted five times with 400 μL of 10 mM maltose in buffer C.

The purified proteins were applied to a Superdex 200 10/300 GL column (GE Healthcare) equilibrated with buffer D (10mM HEPES pH 7.5, 150 mM NaCl, 1 mM DTT, 3 mM EDTA, and 0.05% Tween20) and eluted with the same buffer at a flow rate of 0.5 mL per minute. The peak fraction containing GST-cMYC-SMOS1 or MBP-3xFLAG-SMOS2/DLT was used for surface plasmon resonance (SPR) analysis.

The interaction of immobilized GST-cMYC-SMOS1 protein with MBP-3xFLAG-SMOS2/DLT was assayed by a method based on SPR (Karlsson et al., 2006), using a biosensor instrument (Biacore T100; GE Healthcare, Tokyo, Japan). Binding was measured using the single kinetic method. Anti-GST antibody was immobilized on the CM5 sensor chip using a GST fusion capture kit (GE Healthcare), followed by immobilization of purified GST-cMYC-SMOS1 protein. MBP-3xFLAG-SMOS2/DLT purified as above was used as an analyte. Association and dissociation profiles were obtained using a continuous flow of 30 μL per min. Analyte was applied at concentrations ranging from 0.0625 to 1 μg per mL. Kinetic parameters were obtained using Biacore T100 Evaluation Software v2.

Plant transformation. Each construct was introduced into *Agrobacterium tumefaciens* strain EHA105 and used to infect rice callus, according to Ozawa et al. (2012). Transformed cells and plants were selected by hygromycin resistance, and transgenic plants were grown to maturity in pots under greenhouse conditions.

Microscopy. To observe culm morphology, free-hand sections were cut from the center of each internode of plants at the heading stage, stained with toluidine blue, and viewed by light microscopy. Roots were fixed with formalin: glacial acetic acid: 70 % ethanol (1:1:18) and then dehydrated in a graded ethanol and 1-butanol series. Fixed tissues were embedded in paraplast (McCormic Scientific, LCC, St Louis, MO, USA), cut by a microtome into 8-μm sections and then applied to glass slides. The sections were stained by haematoxylin and observed under a light microscope (BX51; Olympus, Tokyo, Japan). Microtubule orientation

was examined as previously described (Komorisono et al., 2005). Bimolecular Fluorescence Complementation Assay (BiFC) was performed using rice mesophyll protoplasts as previously described (Zhang et al., 2011). YFP fluorescence was recorded by a LSM 700 confocal microscope (Zeiss).

Co-immunoprecipitation. Co-immunoprecipitation was performed as previously described with some modification (Walcher and Nemhauser, 2012; Yang et al., 2014). 2×10^5 isolated mesophyll protoplast were transfected with a total 10 μg of DNA as described in BiFC assay and incubated overnight. Total proteins were extracted from the protoplasts by homogenizing in IP buffer (25 mM Tris-HCl pH8, 1 mM EDTA, 150 mM NaCl, 0.5% Triton X-100, 1x Protease Inhibitor). After centrifugation at 15,000×g for 10 min, 100 μl of supernatant was incubated for 1 hr with 10 μl of dynabeads solution, IP buffer containing protein G dyna-beads (GE Healthcare). The beads were removed by magnetic separation and 2 μl of anti-FLAG M2 (Sigma) were added to the supernatant. After overnight incubation at 4 °C, 10 μl of dynabeads solution was added and incubated for further 4 h at 4 °C. The beads were then washed for five times with 100 μl of IP buffer and samples were analyzed by immunoblot using anti-Flag M2-HRP or anti-HA-HRP antibodies (Sigma).

RNA isolation and expression analysis. Total RNA was extracted using an RNeasy plant mini kit (Qiagen). One μg of total RNA was used to synthesize first-strand cDNA using the Omniscript RT Kit (Qiagen) and oligo (dT) primers. RT-PCR was performed using SsoAdvanced SYBR Green Supermix (Bio-Rad) in a CFX96 Real-Time System (Bio-Rad). A rice ubiquitin gene was used as an internal control. Primer sequences used in this study are listed in Supplementary Table 4.

Transient assay. Calli of cv. Nippponabre or the *smos1-3/smos2-2* double mutant were transferred to fresh N6D solid medium. Particle bombardment was carried out using the PDS-1000/He Biolistic Particle Delivery System (Bio-Rad Laboratories). Plasmid DNA was precipitated onto gold particles (1.6 μm; Bio-Rad Laboratories) by the CaCl2/spermidine method (Klein et al., 1989). The parameters for bombardment were 1350 psi and a microcarrier flight distance of 6 cm. After bombardment, samples were incubated for 16 h in the dark at 30°C. Crude protein extracts of rice calli were prepared on ice by grinding rice calli with a

mortar and pestle in the presence of extraction buffer (100 mM potassium phosphate, pH 7.8, 2 mM DTT, 2 mM EDTA, and 5% (w/v) glycerol). Renilla luciferase (rLUC) activity was assayed using the Renilla Luciferase Assay System (Promega) and firefly luciferase (LUC) activity was assayed using Picagene (Toyo Ink) and measured using a Lumat LB9507 (Berthold technologies), according to the manufacturer's instructions. Firefly LUC (fLUC) expressed under a 35S promoter was used as an internal standard for determining bombardment efficiency, while the rLUC gene was driven by *pOsPHI-1*. Target plasmids and control plasmids were mixed at equivalent molar ratios. The relative specificity of rLUC was calculated by dividing the rLUC activity by the fLUC activity.

Lamina joint bending assay. The lamina joint bending assay by the micro-drop method was performed as described previously with some modification (Hong et al., 2005). Germinated seeds were grown at 30°C for 2 days and ethanol (0.5 μl) containing 1 ng of brassinolide and/or 5 μg of IAA were injected at the top of lamina. After incubating for 3 days, the angle between the lamina and its leaf sheath was measured using IMAGEJ software (http://rsb.info.nih.gov/ij).

Microarray experiments. Agilent 44K rice oligoarrays (Agilent Technologies, Palo Alto, CA, USA), which contain 44,000 features, were used for one-colour oligoarrays. Each feature consists of a 60-mer oligonucleotide corresponding to a full-length cDNA of rice. Total RNA was extracted from the second internodes of rice one day before heading using the RNeasy plant mini kit (Qiagen). Three biological replicate sample sets were analyzed using independently-isolated RNA samples. All microarray experiments were performed according to the manufacturer’s manual. Feature Extraction software (Agilent Technologies) was used to delineate and measure the signal intensity of each spot on the array. The resulting data were normalized using the variance stabilization algorithm (Huber et al., 2002).

Author Contributions

K.H., H.Y., K.A., H.K., M.U-T., and M.M. conceived the project and designed experiments. T.H., K.S-I., and M.H. performed positional cloning of SMOS2/DLT. K.H., H.Y., K.A., M.K., and M.H. did DNA manipulations and phenotypic analyses. M.K. and M.U-T. expressed proteins in *E. coli*, and performed SPR. H.Y., K.A., M.H., M.T-U., and K.H. designed and performed Y2H experiments. M.K., A.K., and K.H. performed the real-time PCR experiments

and transient assays. H.Y. conducted the lamina joint test and co-immunoprecipitaiton analysis. K.H., H.Y., K.A., H.Y., and M.M. wrote the manuscript and M.T-U., K.H., K.A., H.Y., and H.K. revised it.

Acknowledgements

We thank Dr. Yukihisa Shimada and Dr. Ayako Nakamura for providing us the auxin inhibitor PPBo, and Wakana Takase, Satoko Nakamura, Rie Mitani, and Kumiko Furukawa for technical assistance. This work was supported by grants from the Ministry of Agriculture, Forestry and Fisheries of Japan (Genomics-based for Agricultural Improvement, RBS2003) to MM, from KAKENHI (Series of single-year grants, 26･1393) to KH, Grants-in-Aid for Scientific Research on Innovative Areas (No.3806) to M.M., and M. U.-T., and from Grant-in-Aid for JSPS Fellows to HY. The authors declare that they do not have any competing financial interests.

References

Abel, S., Nguyen, M.D., and Theologis, A. (1995). The *PS-IAA4/5*-like family of early auxin-inducible mRNAs in *Arabidopsis thaliana*. J Mol. Biol. **251**: 533-549.

Aya, K., Hobo, T., Sato-Izawa, K., Ueguchi-Tanaka, M., Kitano, H., and Matsuoka, M. (2014). A novel AP2-type transcription factor, SMALL ORGAN SIZE1, controls organ size downstream of an auxin signaling pathway. Plant Cell Physiol. **55**: 897-912.

Bao, F., Shen, J., Brady, S.R., Muday, G.K., Asami, T., and Yang, Z. (2004). Brassinosteroids interact with auxin to promote lateral root development in *Arabidopsis*. Plant Physiol. **34**: 1624-1631.

Clouse, S.D., and Sasse, J.M. (1998). BRASSINOSTEROIDS: Essential Regulators of Plant Growth and Development. Annu. Rev. Plant Physiol. Plant Mol. Biol. **49**: 427-451.

Dunnett, C.W. (1955). A multiple comparison procedure for comparing several treatments with a control. J. of the American Statistical Association **50**: 1096–1121.

Fujioka, S., Noguchi, T., Takatsuto, S., and Yoshida, S. (1998). Activity of brassinosteroids in the dwarf rice lamina inclination bioassay. Phytochemistry **49**: 1841–1848.

Gil, P., Liu, Y., Orbović, V., Verkamp, E., Poff, K.L., and Green, P.J. (1994). Characterization of the auxin-inducible *SAUR-AC1* gene for use as a molecular genetic tool in Arabidopsis. Plant Physiol. **104**: 777-784.

Goda, H., Shimada, Y., Asami, T., Fujioka, S., and Yoshida, S. (2002). Microarray analysis of brassinosteroid-regulated genes in *Arabidopsis*. Plant Physiol. **130**: 1319-1334.

Goda, H., Shimada, Y., Fujioka, S., and Yoshida, S. (2004). Classification of brassinosteroid-regulated genes based on expression profiles in bri1 and in response to a protein kinase inhibitor, staurosporin. Biosci. Biotechnol. Biochem. **68**: 1605-1607.

Hardtke, C.S. (2007). Transcriptional auxin-brassinosteroid crosstalk: who's talking? Bioessays. **29**: 1115-1123.

Hino, T., Tanaka, Y., Kawamukai, M., Nishimura, K., Mano, S., and Nakagawa, T. (2011). Two Sec13p homologs, AtSec13A and AtSec13B, redundantly contribute to the formation of COPII transport vesicles in *Arabidopsis thaliana*. Biosci. Biotechnol. Biochem. **75**: 1848-1852.

Hirano, K., Asano, K., Tsuji, H., Kawamura, M., Mori, H., Kitano, H., Ueguchi-Tanaka, M., and Matsuoka, M. (2010). Characterization of the molecular mechanism underlying gibberellin perception complex formation in rice. Plant Cell **22**: 2680-2696.

Hirano, K., Aya, K., Morinaka, Y., Nagamatsu, S., Sato, Y., Antonio, B.A., Namiki, N., Nagamura, Y., and Matsuoka, M. (2013). Survey of genes involved in rice secondary cell wall formation through a co-expression network. Plant Cell Physiol. **54**: 1803-1821.

Hong, Z., Ueguchi-Tanaka, M., Fujioka, S., Takatsuto, S., Yoshida, S., Hasegawa, Y., Ashikari, M., Kitano, H., and Matsuoka, M. (2005). The Rice *brassinosteroid-deficient*

dwarf2 mutant, defective in the rice homolog of Arabidopsis DIMINUTO/DWARF1, is rescued by the endogenously accumulated alternative bioactive brassinosteroid, dolichosterone. Plant Cell **17**: 2243-2254.

Huber, W., von Heydebreck, A., Sültmann, H., Poustka, A., and Vingron, M. (2002). Variance stabilization applied to microarray data calibration and to the quantification of differential expression. Bioinformatics **18** Suppl 1: S96-104.

Ibañes, M., Fàbregas, N., Chory, J., and Caño-Delgado, A.I. (2009). Brassinosteroid signaling and auxin transport are required to establish the periodic pattern of *Arabidopsis* shoot vascular bundles. Proc. Natl. Acad. Sci. U S A. **106**: 13630-13635.

Inukai, Y., Sakamoto, T., Ueguchi-Tanaka, M., Shibata, Y., Gomi, K., Umemura, I., Hasegawa, Y., Ashikari, M., Kitano, H., and Matsuoka, M. (2005). *Crown rootless1*, which is essential for crown root formation in rice, is a target of an AUXIN RESPONSE FACTOR in auxin signaling. Plant Cell **17**: 1387-1396.

Kakei, Y., Yamazaki, C., Suzuki, M., Nakamura, A., Sato, A., Ishida, Y., Kikuchi, R., Higashi, S., Kokudo, Y., Ishii, T., Soeno, K., and Shimada, Y. (2015). Small molecule auxin inhibitors that target YUCCA are powerful tools for studying auxin function. Plant J. **84**: 827-837.

Karlsson, R., Katsamba, P.S., Nordin, H., Pol, E., and Myszka, D.G. (2006). Analyzing a kinetic titration series using affinity biosensors. Anal. Biochem. **349**: 136-147.

Katsumi, M. (1985). Interaction of a brassinosteroid with IAA and GA_3 in the elongation of cucumber hypocotyl sections. Plant Cell Physiol. **26**: 612-625.

Kim, S-K., Abe, H., Little, C.H.A., and Pharis, R.P. (1990). Identification of two brassinosteroids from the cambial region of scots pine (*Pinus silverstris*) by gas chromatography–mass spectrometry, after detection using a dwarf rice lamina inclination bioassay. Plant Physiol. **94**: 1709–1713.

Klein, T.M., Kornstein, L., Sanford, J.C., and Fromm, M.E. (1989). Genetic transformation of maize cells by particle bombardment. Plant Physiol. **91**: 440-444.

Komorisono, M., Ueguchi-Tanaka, M., Aichi, I., Hasegawa, Y., Ashikari, M., Kitano, H., Matsuoka, M., and Sazuka, T. (2005). Analysis of the rice mutant *dwarf and gladius leaf 1*. Aberrant katanin-mediated microtubule organization causes up-regulation of gibberellin biosynthetic genes independently of gibberellin signaling. Plant Physiol. **138**: 1982-1993.

Lim, S., Park, J., Lee, N., Jeong, J., Toh, S., Watanabe, A., Kim, J., Kang, H., Kim, D.H., Kawakami, N., and Choi, G. (2013). ABA-insensitive3, ABA-insensitive5, and DELLAs interact to activate the expression of *SOMNUS* and other high-temperature-inducible genes in imbibed seeds in *Arabidopsis*. Plant Cell **25**: 4863-4878.

Liu, J.M., Park, S.J., Huang, J., Lee, E.J., Xuan, Y.H., Je, B.I., Kumar, V., Priatama, R.A., Raj K, V., Kim, S.H., et al. (2016). Loose Plant Architecture1 (LPA1) determines lamina joint bending by suppressing auxin signalling that interacts with C-22-hydroxylated and 6-deoxo brassinosteroids in rice. J Exp Bot 67:1883-1895.

Luo, X., Zheng, J., Huang, R., Huang, Y., Wang, H., Jiang, L., and Fang, X. (2016). Phytohormones signaling and crosstalk regulating leaf angle in rice. Plant Cell Rep.

Maeda, E. (1960). Geotropic reaction of excised rice leaves. Physiol Plant 13: 204–213.

Maeda, E. (1961). Studies on the mechanism of leaf formation in crop plants. II. Anatomy of the lamina joint in rice plant. Proc. Soc. Crop Plant Dev. **29**: 234–239.

Maeda, E. (1962). Studies on the mechanism of leaf formation in crop plants. III. Effects of gibberellin on the extension of lamina joints in intact rice seedlings. Proc. Soc. Crop Plant Dev. **31**: 49–54.

Maeda, E. (1965). Rate of lamina inclination in excised rice leaves. Physiol. Plant **18**: 813-

827.

Mandava, N.B. (1988). Plant growth-promoting brassinosteroids. Annu. Rev. Plant Physiol. Plant Mol. Biol. **39**: 23–52.

Millard, C.J., Watson, P.J., Fairall, L., and Schwabe, J.W. (2013). An evolving understanding of nuclear receptor coregulator proteins. J. Mol. Endocrinol. **51**: T23-36.

Müssig, C., Fischer, S., and Altmann, T. (2002). Brassinosteroid-regulated gene expression. Plant Physiol. **129**: 1241-1251.

Nakamura, A., Higuchi, K., Goda, H., Fujiwara, M.T., Sawa, S., Koshiba, T., Shimada, Y., and Yoshida, S. (2003). Brassinolide induces *IAA5, IAA19*, and *DR5*, a synthetic auxin response element in *Arabidopsis*, implying a cross talk point of brassinosteroid and auxin signaling. Plant Physiol. **133**: 1843-1853.

Nemhauser, J.L., Hong, F., and Chory, J. (2006). Different plant hormones regulate similar processes through largely nonoverlapping transcriptional responses. Cell 126: 467-475.

Nemhauser, J.L., Mockler, T.C., and Chory, J. (2004). Interdependency of brassinosteroid and auxin signaling in *Arabidopsis*. PLoS Biol. **2**: E258.

Oh, E., Zhu, J.Y., Bai, M.Y., Arenhart, R.A., Sun, Y., and Wang, Z.Y. (2014). Cell elongation is regulated through a central circuit of interacting transcription factors in the *Arabidopsis* hypocotyl. Elife **3**.

Ohta, S., Mita, S., Hattori, T., and Nakamura, K. (1990). Construction and expression in tobacco of a *β-Glucuronidase (GUS)* reporter gene containing an intron within the coding sequence. Plant Cell Physiol. **31**: 805-813.

Oshima, Y., Mitsuda, N., Nakata, M., Nakagawa, T., Nagaya, S., Kato, K., and Ohme-

Takagi, M. (2011). Novel vector systems to accelerate functional analysis of transcription factors using chimeric repressor gene-silencing technology (CRES-T). Plant Biotechnol. **28**: 201–210.

Ozawa, K. (2012). A high-efficiency *Agrobacterium*-mediated transformation system of rice (*Oryza sativa L.*). Methods Mol. Biol. **847**: 51-57.

Park, T., Cho, H., Hwang, I., and Choe, S. (2011). Auxin stimulates *DWARF4* expression and brassinosteroid biosynthesis in *Arabidopsis*. Plant J. **66**: 564-578.

Perrot-Rechenmann, C. (2010). Cellular responses to auxin: division versus expansion. Cold Spring Harb. Perspect. Biol. 2: a001446.

Sakamoto, T., Ohnishi, T., Fujioka, S,, Watanabe, B., and Mizutani, M. (2012). Rice CYP90D2 and CYP90D3 catalyze C-23 hydroxylation of brassinosteroids *in vitro*. Plant Physiol. Biochem. **58**: 220-226.

Schröder, F., Lisso, J., Lange, P., and Müssig, C. (2009). The extracellular EXO protein mediates cell expansion in *Arabidopsis* leaves. BMC Plant Biol. **9**: 20.

Sun, S., Chen, D., Li, X., Qiao, S., Shi, C., Li, C., Shen, H., and Wang, X. (2015). Brassinosteroid signaling regulates leaf erectness in *Oryza sativa* via the control of a specific U-type cyclin and cell proliferation. Dev. Cell **34**: 220-228.

Sun, X., Jones, W.T., and Rikkerink, E.H. (2012). GRAS proteins: the versatile roles of intrinsically disordered proteins in plant signalling. Biochem. J. **442**: 1-12.

Sun, Y., Yang, Y., Yuan, Z., Müller, J.L., Yu, C., Xu, Y., Shao, X., Li, X., Decker, E.L., Reski, R., and Huang, H. (2010). Overexpression of the *Arabidopsis* gene *UPRIGHT ROSETTE* reveals a homeostatic control for indole-3-acetic acid. Plant Physiol. **153**: 1311-1320.

Takeno, K., and Pharis, R.P. (1982). Brassinosteroid-induced bending of the leaf lamina of

dwarf rice seedlings: an auxin-mediated phenomenon. Plant Cell Physiol. **23**, 1275-1281.

Tian, C., Wan, P., Sun, S., Li, J., and Chen, M. (2004). Genome-wide analysis of the GRAS gene family in rice and *Arabidopsis*. Plant Mol. Biol. **54**: 519-532.

Tong, H., Jin, Y., Liu, W., Li, F., Fang, J., Yin, Y., Qian, Q., Zhu, L., and Chu, C. (2009). DWARF AND LOW-TILLERING, a new member of the GRAS family, plays positive roles in brassinosteroid signaling in rice. Plant J. **58**: 803-816.

Tong, H., Liu, L., Jin, Y., Du, L., Yin, Y., Qian, Q., Zhu, L,, and Chu, C. (2012). DWARF AND LOW-TILLERING acts as a direct downstream target of a GSK3/SHAGGY-like kinase to mediate brassinosteroid responses in rice. Plant Cell **24**: 2562-2577.

Ueguchi-Tanaka, M., Ashikari, M., Nakajima, M., Itoh, H., Katoh, E., Kobayashi, M., Chow, T.Y., Hsing, Y.I., Kitano, H., Yamaguchi, I., and Matsuoka, M. (2005). *GIBBER-ELLIN INSENSITIVE DWARF1* encodes a soluble receptor for gibberellin. Nature 437: 693-698.

Varlakhanova, N., Hahm, J.B., and Privalsky, M.L. (2011). Regulation of SMRT core-pressor dimerization and composition by MAP kinase phosphorylation. Mol. Cell Endocrinol. **332**: 180-188.

Walcher, C.L., and Nemhauser, J.L. (2012). Bipartite promoter element required for auxin response. Plant Physiol. **158**: 273-282.

Woodward, A.W., and Bartel, B. (2005). Auxin: regulation, action, and interaction. Ann. Bot. **95**: 707-735.

Wright, R.C., and Nemhauser, J.L. (2015). New tangles in the auxin signaling web. F1000Prime Rep. **7**: 19.

Yang, J.W., Fu, J.X., Li, J., Cheng, X.L., Li, F., and Dong, J.F. (2014). A Novel Co-immunoprecipitation protocol based on protoplast transient gene expression for studying protein-protein interactions in rice. Plant Mol. Biol. Rep. **32**: 153-161.

Yin, Y., Wang, Z.Y., Mora-Garcia, S., Li, J., Yoshida, S., Asami, T., and Chory, J. (2002). BES1 accumulates in the nucleus in response to brassinosteroids to regulate gene expression and promote stem elongation. Cell **109**: 181-191.

Yokota, T., and Mori, K. (1992). Molecular structure and biological activity of brassinolide and related (brassino)steroids. In Molecular Structure and Biological Activity of Steroids (eds. by Duax, W.L. & Bohl, M.) 317–340 (CRC Press. CRC Press, Boca Raton, FL).

Yopp, J.H., Mandava, N.B., and Sasse, J.M. (1981). Brassinolide, a growth-promoting steroidal lactone. I. Activity in selected auxin bioassays. Physiol. Plant **53**: 445-452.

Yoshida, H., Hirano, K., Sato, T., Mitsuda, N., Nomoto, M., Maeo, K., Koketsu, E., Mitani, R., Kawamura, M., Ishiguro, S., Tada, Y., Ohme-Takagi, M., Matsuoka, M., and Ueguchi-Tanaka, M. (2014). DELLA protein functions as a transcriptional activator through the DNA binding of the indeterminate domain family proteins. Proc. Natl. Acad. Sci. USA **111**: 7861–7866.

Yoshida, H., Ueguchi-Tanaka, M., and Matsuoka, M. (2014). Regulatory Networks Acted Upon by the GID1-DELLA System After Perceiving Gibberellin. Enzymes **35**: 1-25.

Yoshimitsu, Y., Tanaka, K., Fukuda, W., Asami, T., Yoshida, S., Hayashi, K., Kamiya, Y., Jikumaru, Y., Shigeta, T., Nakamura, Y., Matsuo, T., and Okamoto, S. (2011). Transcription of *DWARF4* plays a crucial role in auxin-regulated root elongation in addition to brassinosteroid homeostasis in *Arabidopsis thaliana*. PLoS One **6**: e23851.

Zhang, Y., Su, J., Duan, S., Ao, Y., Dai, J., Liu, J., Wang, P., Li, Y., Liu, B., Feng, D., Wang, J., and Wang, H. (2011). A highly efficient rice green tissue protoplast system for transient gene expression and studying light/chloroplast-related processes. Plant Methods **7**:

30.

Zhu, J.Y., Sae-Seaw, J., and Wang, Z.Y. (2013). Brassinosteroid signalling. Development **140**: 1615-1620.

Figure Legends

Figure 1. Phenotypes of *smos* mutants. (**A**) Gross morphology of plants grown in the field at the heading stage. T65 is the original cultivar of *smos1-1*, and Nipponbare is the original cultivar of other *smos* mutants. Scale bar, 30 cm. (**B**) Diagram of plant height. (**C**) Cross sections of the second internode. Scale bars, 200 μm. (**D**) Culm thickness of each internode. (**E**) Cell density of the second internode. (**F**) Comparison of gene expression between *smos1-3* and *smos2-2*. Gene expression in each mutant was divided by the expression in wild type Nipponbare. The RNA used for microarray analysis was extracted from the second internodes of WT, *smos1-3*, and *smos2-2* one day before heading. The y-axis represents the log2 ratio of the signal intensity of corresponding probes in *smos2-2* and WT, whereas the x-axis shows that of *smos1-3*. More than three biological replicates were analyzed for **B**, **D** and **E** (means ± SD). Two asterisks in **B**, **D** and **E** indicate statistically significant differences in comparison to the WT ($P < 0.01$) (Dunnett, 1955). **B**, **D** and **E** were generated from the data shown in Supplementary Table 1.

Figure 2. Cloning of *SMOS2*. (**A**) The *SMOS2* locus was detected between markers D38 and RM276 on chromosome 6. A fine-mapping strategy was used to localize *SMOS2* to a 22.6-kb region between markers SNP038 and RM586. Numbers under the map indicate the number of recombinants. The candidate region was narrowed down to seven genes according to RAP-DB (shown as arrows, http://rapdb.dna.affrc.go.jp). (**B**) Schematic structure of the SMOS2 protein. The line before the box indicates the 5' untranslated region. *smos2-1* has a 510-bp deletion encompassing the 5' untranslated and N-terminal coding regions, whereas *smos2-2* has a 1-bp insertion in the VHIID domain. The insertion in *smos2-2* and the resulting amino acid changes around the mutation site are shown in red font. (**C**) Complementation analysis of *smos2-1* after the introduction of a 6.5-kb genomic fragment containing *SMOS2* and its 5' and 3' flanking regions. The plants were grown under greenhouse conditions. Scale bar, 20 cm.

Figure 3. Interaction between SMOS1 and SMOS2/DLT. (**A**) The interaction between SMOS1 and SMOS2/DLT proteins in yeast. *β-galactosidase* (β-Gal) activity was measured in a liquid assay to indicate binding activity (means ± SD; n = 3). SMOS1 was used as the bait, and SMOS2/DLT was used as the prey. (**B**) Physicochemical analysis of the interaction

between SMOS1 and SMOS2/DLT measured by surface plasmon resonance (SPR). The left panel shows the interaction between GST-cMYC and MBP-3xFLAG-SMOS2/DLT (negative control). The right panel shows the interaction between GST-cMYC-SMOS1 and MBP-3xFLAG (negative control, SMOS1), and GST-cMYC-SMOS1 and MBP-3xFLAG-SMOS2/DLT (SMOS1+SMOS2). (**C**) Rice mesophyll protoplasts were transfected to express SMOS1-HA or SMOS2-FLAG alone or co-transfected, and the extracted proteins were immunoprecipitated by anti-FLAG antibody. Gel blots were probed with anti-FLAG or anti-HA antibody. (**D**) Transactivation activities of SMOS1 and SMOS2/DLT in yeast. SMOS1 or SMOS2/DLT were fused with the GAL4 DNA-binding domain and β-Gal activity was quantified in the presence or absence of SMOS2/DLT and SMOS1, respectively (means ± SD; n = 3).

Figure 4. SMOS1 cannot rescue the mutant phenotype of *smos1-3*/*smos2-2*. (**A**) Over-expression of *SMOS1-SRDX* mimics the *smos* phenotype. A control plant (empty vector introduced Nipponbare) is shown on the left and Nipponbare over-expressing *SMOS1-SRDX* is shown on the right. Scale bar, 20 cm. (**B**) Transverse sections of leaf sheaths from plants transformed with empty vector (left) or *pAct:SMOS1-SRDX* (right). Asterisks indicate cells with irregular and small shape. Scale bar, 50 μm. (**C**) Cross sections of culms from plants transformed with empty vector (left) or *pAct:SMOS1-SRDX* (right). Scale bar, 200 μm. (**D**) Gross morphology of transgenic plants over-expressing *SMOS1* in *smos1-3* and *smos1-3/smos2-2* mutant backgrounds. From the left: vector introduced Nipponbare control, vector introduced in *smos1-3*, *SMOS1* over-expressed in *smos1-3*, vector only in *smos1-3/smos2-2*, and *SMOS1* over-expressed in *smos1-3/smos2-2*. Scale bar, 20 cm. (**E**) Transverse sections of the third internode of the plants in **D**. Scale bar, 100 μm. (**F**) Microtubule orientation of plants shown in **D**. Scale bar, 20 μm.

Figure 5. Both SMOS1 and SMOS2/DLT are required to enhance the expression of the *OsPHI-1* gene. (**A**) *OsPHI-1* expression in WT and *smos* mutants. 10-day-old seedlings cut 1 cm from the base were used for the analysis (means ± SD; n = 3). (**B**) Effect of *SMOS1* over-expression on *OsPHI-1* expression in *smos1-3* and *smos1-3/smos2-2* mutants. Second internodes collected one day before heading were used for the analysis (means ± SD; n = 3). Relative *OsPHI-1* expression was calculated by dividing by the Ubiquitin expression in (A) and

(B). pAct/pUC19 was used as a vector control (Vec). (**C**) Transient assay to examine the effect of SMOS1 and SMOS2/DLT on *OsPHI-1* expression in rice callus. Schematics of the effector, reporter, and internal control constructs are drawn on the left-hand side. *pAct*-driven *SMOS1* and/or *SMOS2/DLT*, and 35S-driven *firefly LUC (fLUC)* were co-expressed with *pOsPHI-1*-driven *rennila LUC (rLUC)*. Relative rLUC activity was calculated by dividing by the fLUC activity. *pAct*/pUC19 was used as a vector control. Three-week-old *smos1-3/smos2-2* double mutant callus was used. Data represent the average value ± SE of at least three replicates. One asterisk in **c,** and two asterisks in **A**, **B** and **C** indicate statistically significant differences in comparison to the WT or vector control ($P < 0.05$ and $P < 0.01$, respectively) (Dunnett, 1955). n.s indicates no significant difference compared to vector control.

Figure 6. The SMOS1-SMOS2 interaction occurs via the C-terminal conserved motif of SMOS1. (**A**) Schematic structure of the SMOS1 protein. The AP2 DNA-binding domain and the conserved SMOS1 family motifs reported by Aya et al. (2014) are presented. (**B**) The interaction of DB-fused SMOS2/DLT and AD-fused SMOS1 with a deletion in each motif were analyzed in yeast. β-Gal activity was measured in yeast (means ± SD; n = 3). (**C**) Transient assay of *OsPHI-1* expression by various SMOS1 deletions. Experimental procedures were the same as those used for Fig 5C. (**D**) BiFC analysis of the in vivo interaction between SMOS1 and SMOS2/DLT, or ΔWTNF SMOS1 and SMOS2/DLT in rice protoplasts. (**E**) Over-expression of ΔWTNF SMOS1 could not rescue the dwarf phenotype of *smos1-3*. Scale bar, 20 cm. (**F**) Transverse sections of the third internode of plants in **e**. Scale bar, 200 μm.

Figure 7. Effect of auxin, the auxin inhibitor PPBo, BL, and IAA3 on the expression of *SMOS1*, *SMOS2*/*DLT*, and *OsPHI-1*. (**A**) Proposed model of *OsPHI-1* expression in rice. (**B**) Expression of *OsPHI-1* in WT, *smos1-3*, and *smos2-2* rice treated with BL. (**C**) Expression of *SMOS1* in WT and *smos1-3* treated with BL. (**D**) Expression of *OsPHI-1* in WT treated with IAA at various time points. (**E-G**) Expression of *SMOS1* (**E**), *OsPHI-1* (**F**) and *SMOS2*/*DLT* (**G**) in WT rice treated with PPBo. (**H-J**) Expression of *SMOS1* (**H**), *OsPHI-1* (**I**) and *SMOS2*/*DLT* (**J**) in *IAA P58L* over-expressed rice. RT-PCR analysis was conducted for each experiment (means ± SD; n = 3). Plants were grown for 10 days and seedlings cut 1 cm from the base were used for the analysis. The expression of mock-treated WT was set to 1 in

each panel. n.s indicates no significant difference compared to WT or mock treated rice. (**K**) Lamina joint bending test of *smos* mutants. Addition of auxin and/or BL increase the lamina joint bending angle of WT, while *smos* mutants show attenuated bending compared to WT. PPBo; p-phenoxyphenyl boronic acid. One asterisk and two asterisks indicate statistically significant differences in comparison to the WT or mock treated rice ($P < 0.05$ and $P < 0.01$, respectively) (Dunnett, 1955).

Supplementary Figure 1. Root morphology and cellular organization of roots and leaf sheaths of *smos1* and *smos2* mutants. (**A**) Roots of *smos1-1* and its original cultivar T65, *smos2-1* and its original cultivar Nipponbare. Blue, red, and green lines indicate elongation, transition, and divisional zones, respectively. Scale bars, 200 μm. (**B**) Close up view of the red boxes in the roots in **A**. Scale bar, 20 μm. (**C**) Transverse sections of leaf sheaths. Scale bar, 50 μm. Red arrowheads show cells with irregular and small shape.

Supplementary Figure 2. Complementation analysis of *smos2-2* after the introduction of a 6.5-kb genomic fragment containing *SMOS2* and its 5' and 3' flanking regions.
The plants were grown under greenhouse conditions. Scale bar, 20cm.

Supplementary Figure 3. Expression patterns of *SMOS1* and *SMOS2*/*DLT* in various organs and developmental stages. Note that *SMOS1* and *SMOS2*/*DLT* have similar expression patterns. Expression data were obtained from RiceXpro (http://ricexpro.dna.affrc.go.jp/GGEP/index.html).

Supplementary Figure 4. Effect of auxin and the auxin inhibitor PPBo on the expression of *IAA3* and *OsPHI-1*. (**A**) Expression of *OsIAA3* (**A**) in WT rice treated with IAA. (**B**) Expression of *OsIAA3* in WT rice treated with PPBo. One asterisk and two asterisks indicate statistically significant differences in comparison to mock treated rice ($P < 0.05$ and $P < 0.01$, respectively) (Dunnett, 1955). n.s indicates no significant difference compared to mock treated plant.

Supplementary Figure 5. SMOS1 can interact with GRAS proteins other than SMOS2/DLT. The interactions between SMOS1 and GRAS proteins in yeast. SMOS1 was

used as bait, and GRAS proteins were used as prey. Red font indicates the GRAS proteins that interact with SMOS1. −TL, synthetic complete medium lacking Trp and Leu; −TLH +3-AT, synthetic complete medium lacking Trp, Leu, and His with added 5 mM 3-AT, 3-aminotriazole, which is a competitive inhibitor of the HIS3 enzyme; –TLA, synthetic complete medium lacking Trp, Leu, and Ala.

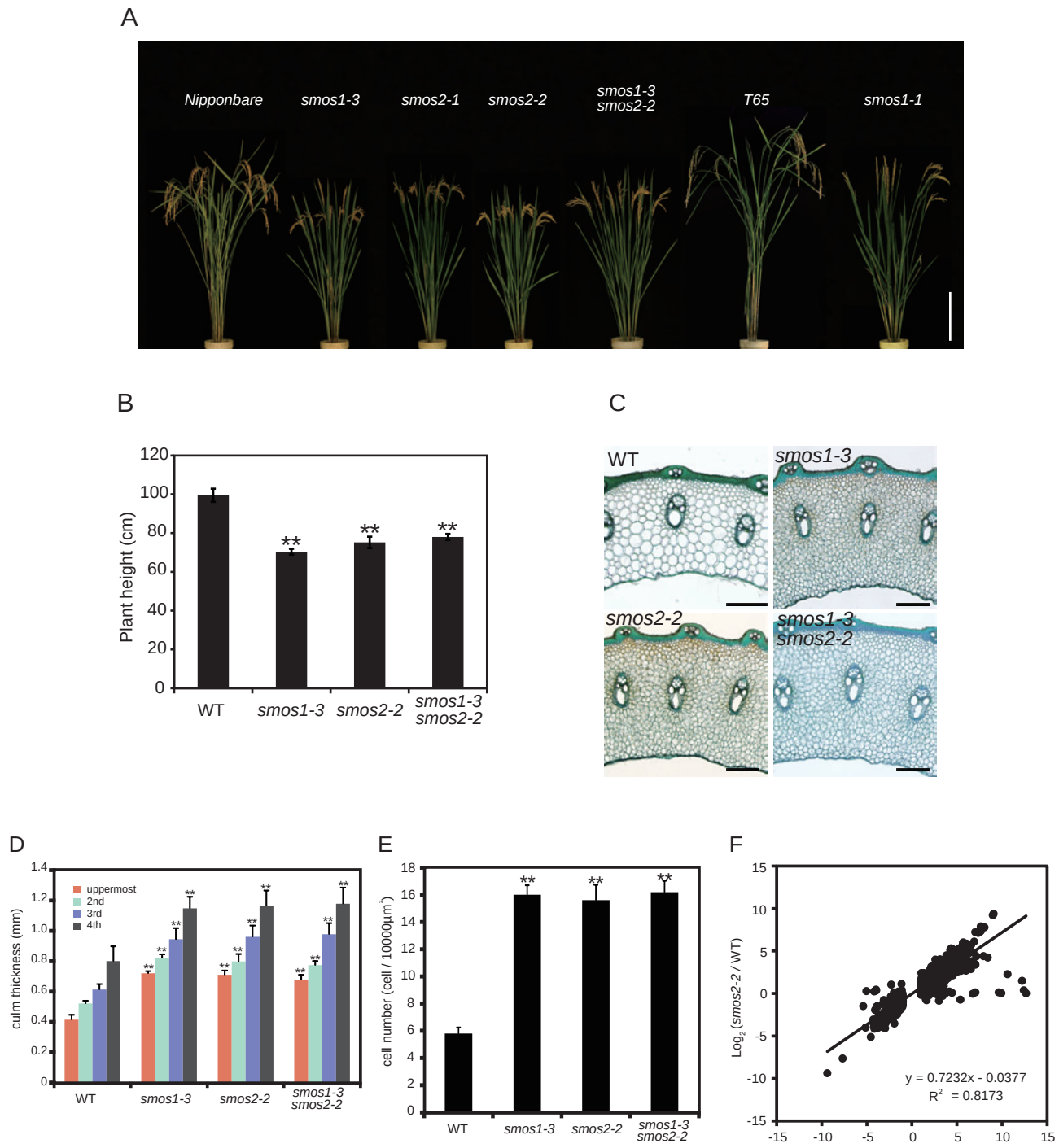

Figure 1. Phenotypes of *smos* mutants. (**A**) Gross morphology of plants grown in the field at the heading stage. T65 is the original cultivar of *smos1-1*, and Nipponbare is the original cultivar of other *smos* mutants. Scale bar, 30 cm. (**B**) Diagram of plant height. (**C**) Cross sections of the second internode. Scale bars, 200 μm. (**D**) Culm thickness of each internode. (**E**) Cell density of the second internode. (**F**) Comparison of gene expression between *smos1-3* and *smos2-2*. Gene expression in each mutant was divided by the expression in wild type Nipponbare. The RNA used for microarray analysis was extracted from the second internodes of WT, *smos1-3*, and *smos2-2* one day before heading. The y-axis represents the log2 ratio of the signal intensity of corresponding probes in *smos2-2* and WT, whereas the x-axis shows that of *smos1-3*. More than three biological replicates were analyzed for **B**, **D** and **E** (means ± SD). Two asterisks in **B**, **D** and **E** indicate statistically significant differences in comparison to the WT ($P < 0.01$) (Dunnett, 1955). **B**, **D** and **E** were generated from the data shown in Supplementary Table 1.

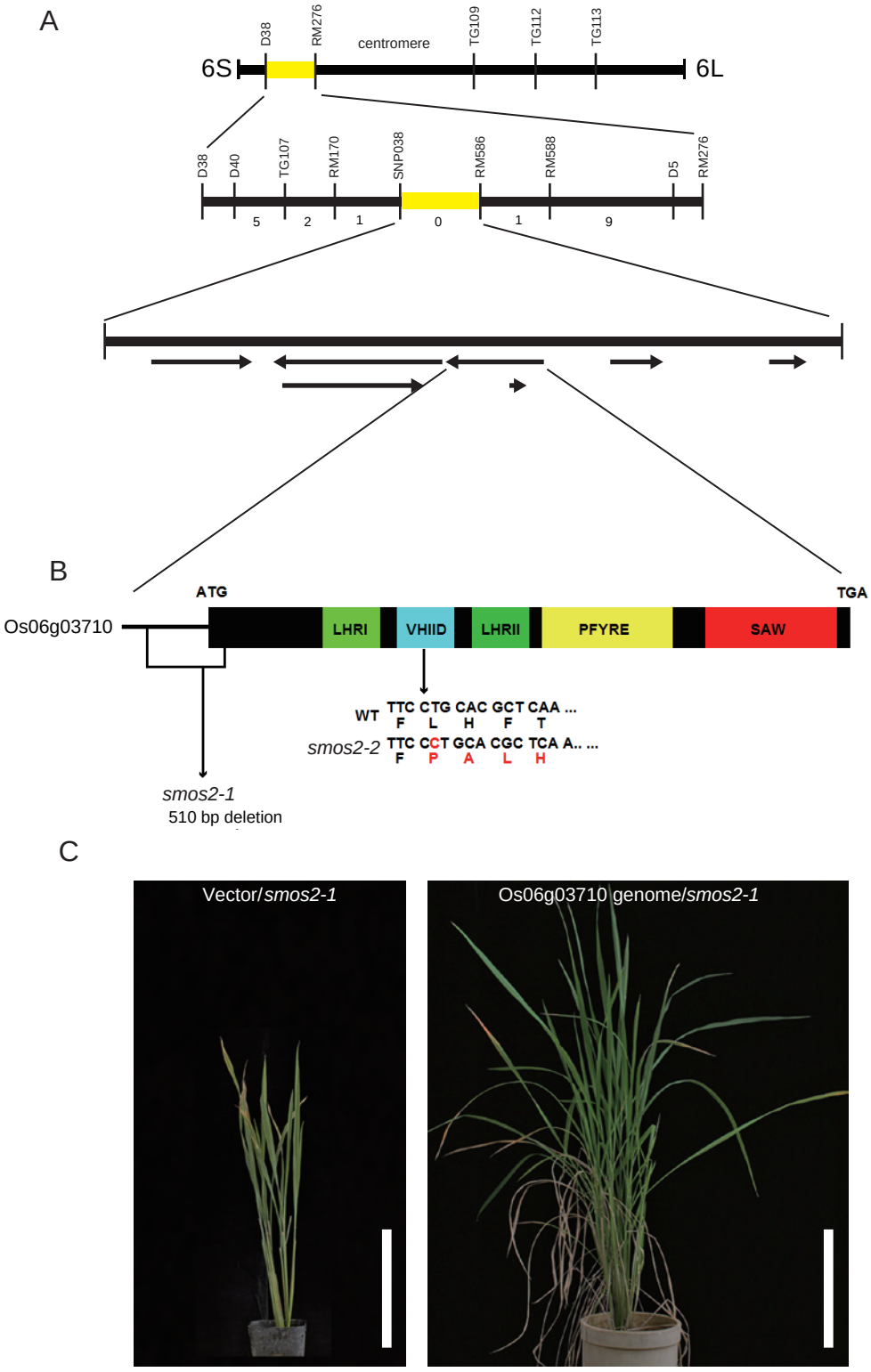

Figure 2. Cloning of *SMOS2*. (**A**) The *SMOS2* locus was detected between markers D38 and RM276 on chromosome 6. A fine-mapping strategy was used to localize *SMOS2* to a 22.6-kb region between markers SNP038 and RM586. Numbers under the map indicate the number of recombinants. The candidate region was narrowed down to seven genes according to RAP-DB (shown as arrows, http://rapdb.dna.affrc.go.jp). (**B**) Schematic structure of the SMOS2 protein. The line before the box indicates the 5' untranslated region. *smos2-1* has a 510-bp deletion encompassing the 5' untranslated and N-terminal coding regions, whereas *smos2-2* has a 1-bp insertion in the VHIID domain. The insertion in *smos2-2* and the resulting amino acid changes around the mutation site are shown in red font. (**C**) Complementation analysis of *smos2-1* after the introduction of a 6.5-kb genomic fragment containing *SMOS2* and its 5' and 3' flanking regions. The plants were grown under greenhouse conditions. Scale bar, 20 cm.

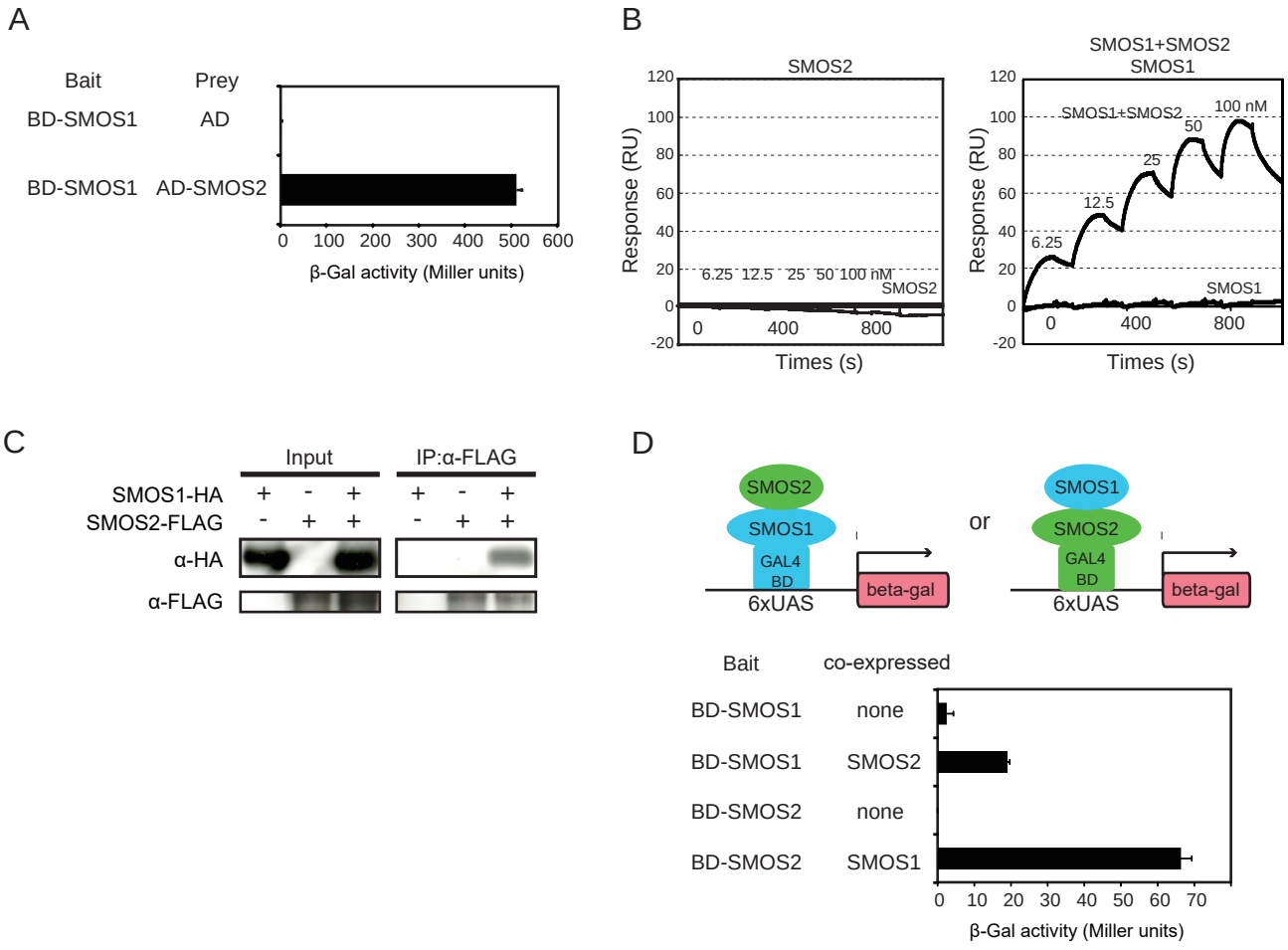

Figure 3. Interaction between SMOS1 and SMOS2/DLT. (**A**) The interaction between SMOS1 and SMOS2/DLT proteins in yeast. *β-galactosidase* (β-Gal) activity was measured in a liquid assay to indicate binding activity (means ± SD; n = 3). SMOS1 was used as the bait, and SMOS2/DLT was used as the prey. (**B**) Physicochemical analysis of the interaction between SMOS1 and SMOS2/DLT measured by surface plasmon resonance (SPR). The left panel shows the interaction between GST-cMYC and MBP-3xFLAG-SMOS2/DLT (negative control). The right panel shows the interaction between GST-cMYC-SMOS1 and MBP-3xFLAG (negative control, SMOS1), and GST-cMYC-SMOS1 and MBP-3xFLAG-SMOS2/DLT (SMOS1+SMOS2). (**C**) Rice mesophyll protoplasts were transfected to express SMOS1-HA or SMOS2-FLAG alone or co-transfected, and the extracted proteins were immunoprecipitated by anti-FLAG antibody. Gel blots were probed with anti-FLAG or anti-HA antibody. (**D**) Transactivation activities of SMOS1 and SMOS2/DLT in yeast. SMOS1 or SMOS2/DLT were fused with the GAL4 DNA-binding domain and β-Gal activity was quantified in the presence or absence of SMOS2/DLT and SMOS1, respectively (means ± SD; n = 3).

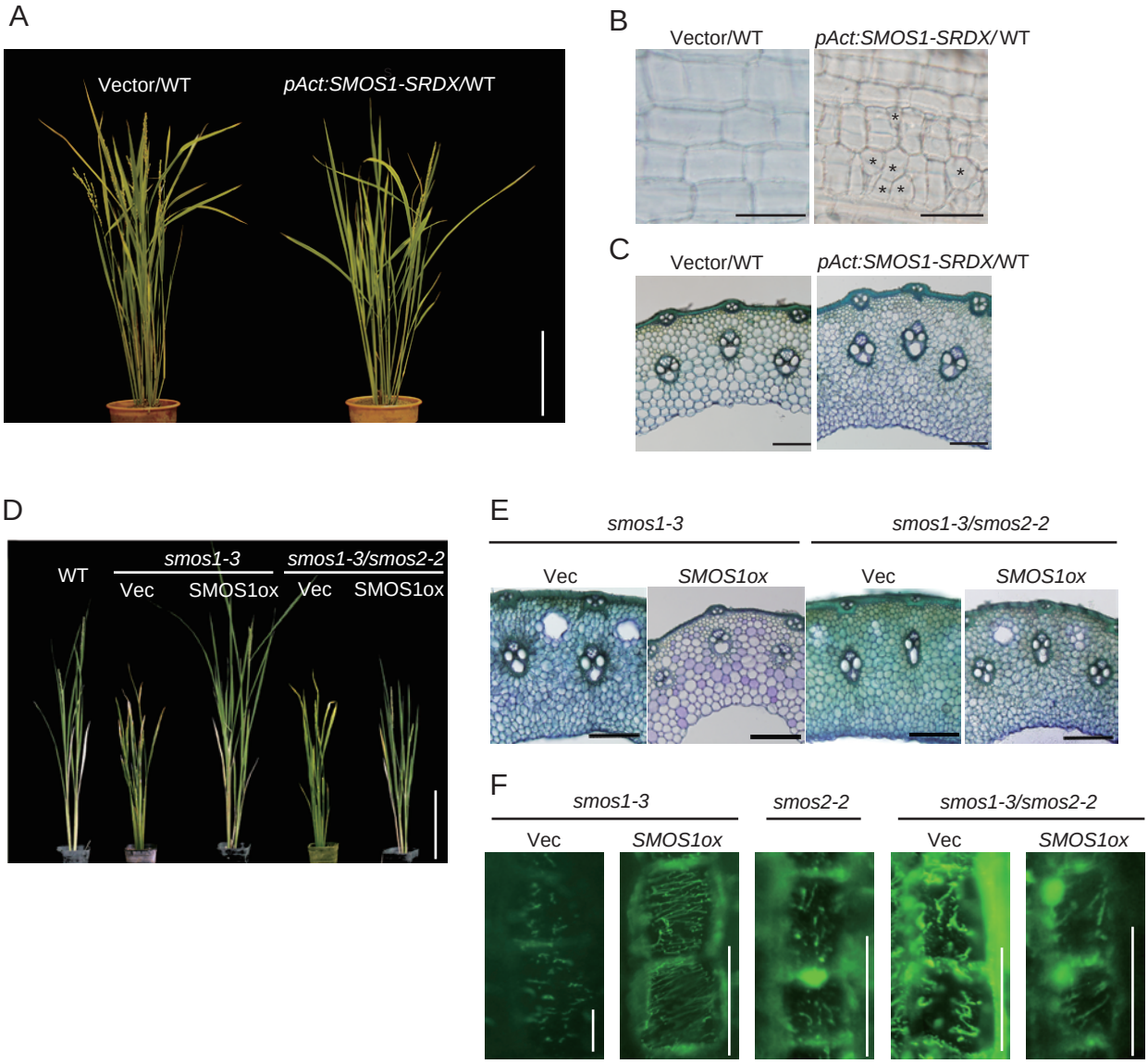

Figure 4. SMOS1 cannot rescue the mutant phenotype of *smos1-3*/*smos2-2*. (**A**) Over-expression of *SMOS1-SRDX* mimics the *smos* phenotype. A control plant (empty vector introduced Nipponbare) is shown on the left and Nipponbare over-expressing *SMOS1-SRDX* is shown on the right. Scale bar, 20 cm. (**B**) Transverse sections of leaf sheaths from plants transformed with empty vector (left) or *pAct:SMOS1-SRDX* (right). Asterisks indicate cells with irregular and small shape. Scale bar, 50 μm. (**C**) Cross sections of culms from plants transformed with empty vector (left) or *pAct:SMOS1-SRDX* (right). Scale bar, 200 μm. (**D**) Gross morphology of transgenic plants over-expressing *SMOS1* in *smos1-3* and *smos1-3/smos2-2* mutant backgrounds. From the left: vector introduced Nipponbare control, vector introduced in *smos1-3*, *SMOS1* over-expressed in *smos1-3*, vector only in *smos1-3/smos2-2*, and *SMOS1* over-expressed in *smos1-3/smos2-2*. Scale bar, 20 cm. (**E**) Transverse sections of the third internode of the plants in **D**. Scale bar, 100 μm. (**F**) Microtubule orientation of plants shown in **D**. Scale bar, 20 μm.

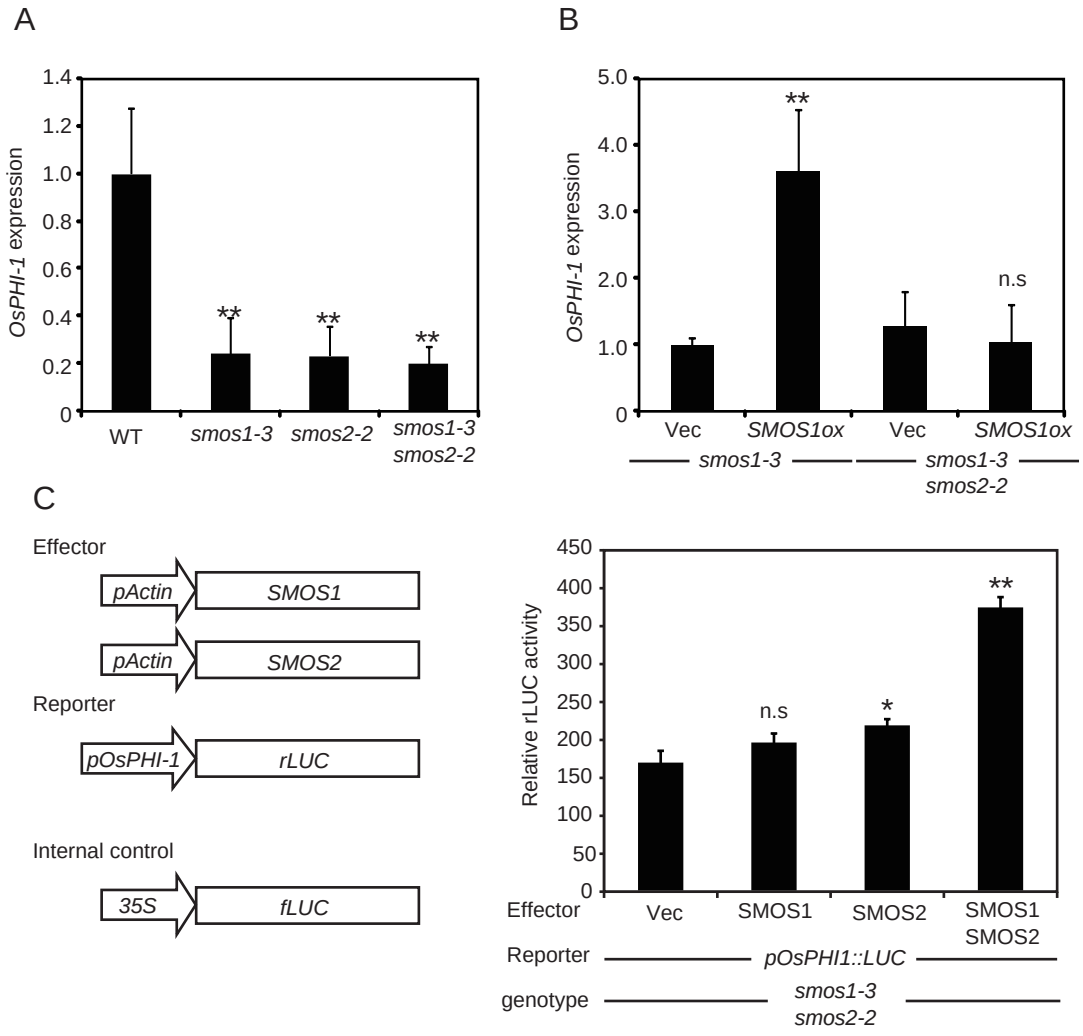

Figure 5. Both SMOS1 and SMOS2/DLT are required to enhance the expression of the *OsPHI-1* gene. (**A**) *OsPHI-1* expression in WT and *smos* mutants. 10-day-old seedlings cut 1 cm from the base were used for the analysis (means ± SD; n = 3). (**B**) Effect of *SMOS1* overexpression on *OsPHI-1* expression in *smos1-3* and *smos1-3/smos2-2* mutants. Second internodes collected one day before heading were used for the analysis (means ± SD; n = 3). Relative *OsPHI-1* expression was calculated by dividing by the Ubiquitin expression in (A) and (B). pAct/pUC19 was used as a vector control (Vec). (**C**) Transient assay to examine the effect of SMOS1 and SMOS2/DLT on *OsPHI-1* expression in rice callus. Schematics of the effector, reporter, and internal control constructs are drawn on the left-hand side. *pAct*-driven *SMOS1* and/or *SMOS2/DLT*, and 35S-driven *firefly LUC (fLUC)* were co-expressed with *pOsPHI-1*-driven *rennila LUC (rLUC)*. Relative rLUC activity was calculated by dividing by the fLUC activity. *pAct*/pUC19 was used as a vector control. Three-week-old *smos1-3/smos2-2* double mutant callus was used. Data represent the average value ± SE of at least three replicates. One asterisk in **c,** and two asterisks in **A**, **B** and **C** indicate statistically significant differences in comparison to the WT or vector control ($P < 0.05$ and $P < 0.01$, respectively) (Dunnett, 1955). n.s indicates no significant difference compared to vector control.

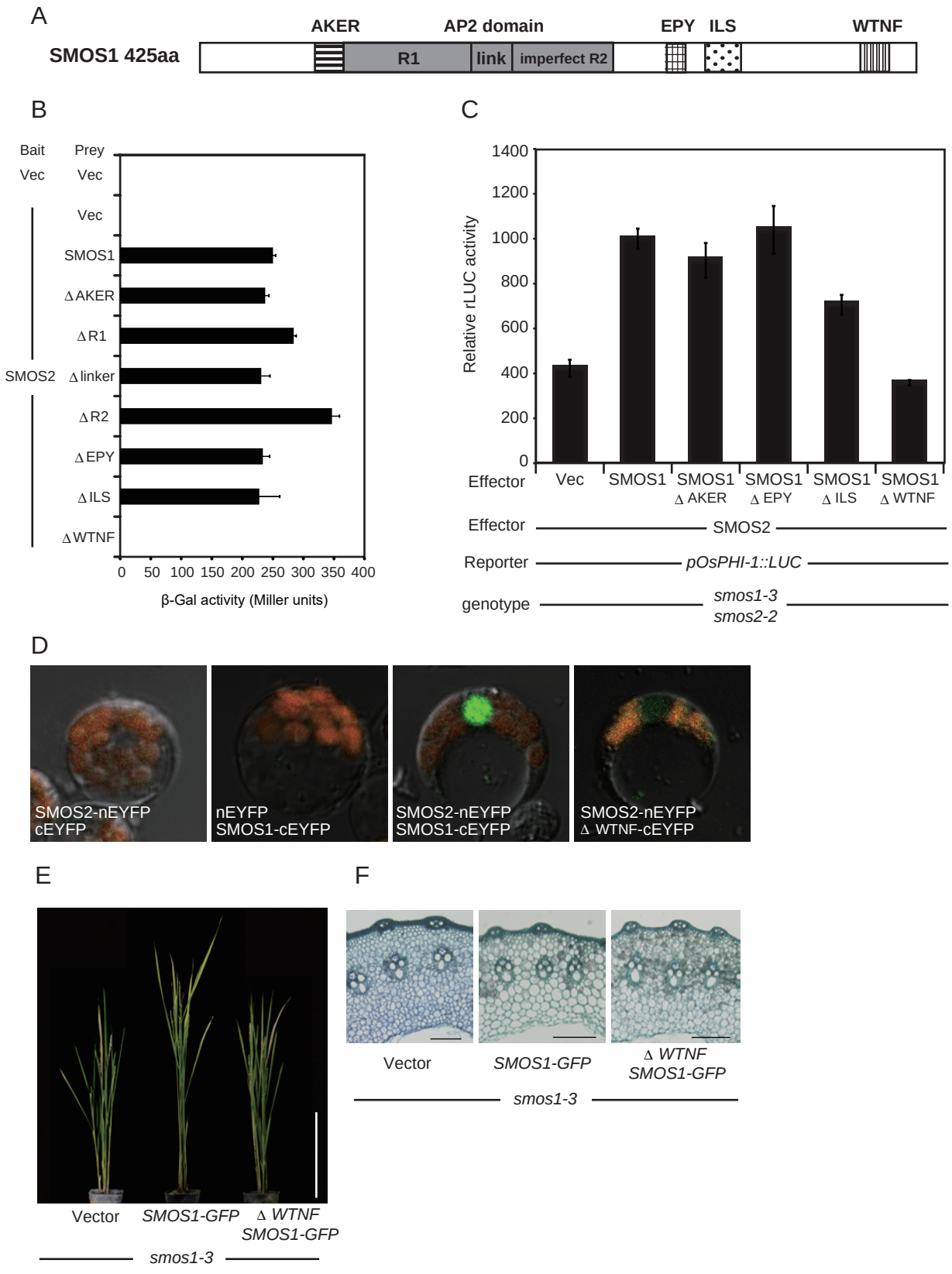

Figure 6. The SMOS1-SMOS2 interaction occurs via the C-terminal conserved motif of SMOS1. (**A**) Schematic structure of the SMOS1 protein. The AP2 DNA-binding domain and the conserved SMOS1 family motifs reported by Aya et al. (2014) are presented. (**B**) The interaction of DB-fused SMOS2/DLT and AD-fused SMOS1 with a deletion in each motif were analyzed in yeast. β-Gal activity was measured in yeast (means ± SD; n = 3). (**C**) Transient assay of *OsPHI-1* expression by various SMOS1 deletions. Experimental procedures were the same as those used for Fig 5C. (**D**) BiFC analysis of the in vivo interaction between SMOS1 and SMOS2/DLT, or ΔWTNF SMOS1 and SMOS2/DLT in rice protoplasts. (**E**) Over-expression of ΔWTNF SMOS1 could not rescue the dwarf phenotype of *smos1-3*. Scale bar, 20 cm. (**F**) Transverse sections of the third internode of plants in **e**. Scale bar, 200 μm.

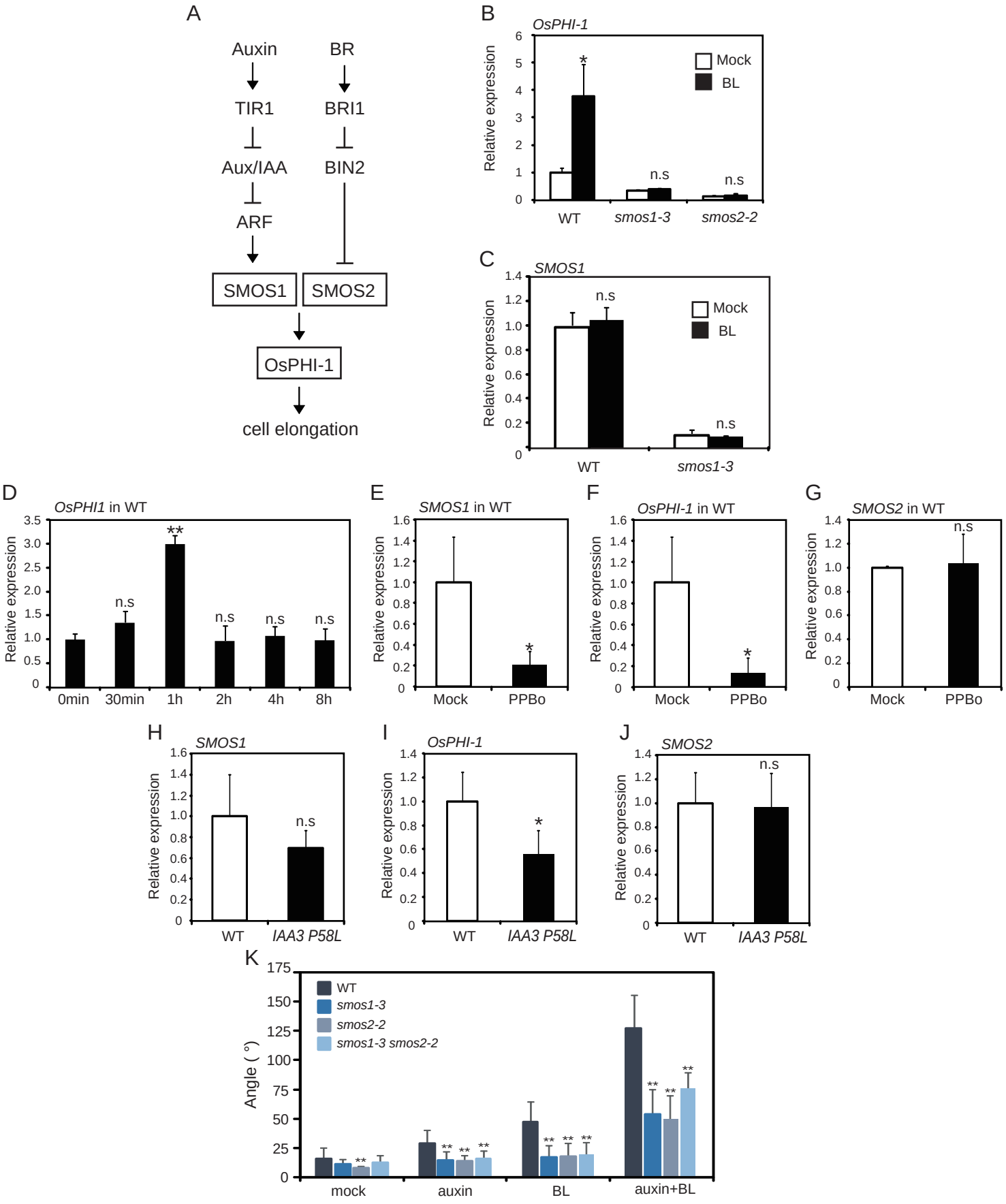

Figure 7. Effect of auxin, the auxin inhibitor PPBo, BL, and IAA3 on the expression of *SMOS1*, *SMOS2*/*DLT*, and *OsPHI-1*. (**A**) Proposed model of *OsPHI-1* expression in rice. (**B**) Expression of *OsPHI-1* in WT, *smos1-3*, and *smos2-2* rice treated with BL. (**C**) Expression of *SMOS1* in WT and *smos1-3* treated with BL. (D) Expression of *OsPHI-1* in WT treated with IAA at various time points. (**E-G**) Expression of *SMOS1* (**E**), *OsPHI-1* (**F**) and *SMOS2*/*DLT* (**G**) in WT rice treated with PPBo. (**H-J**) Expression of *SMOS1* (**H**), *OsPHI-1* (**I**) and *SMOS2*/*DLT* (**J**) in *IAA P58L* over-expressed rice. RT-PCR analysis was conducted for each experiment (means ± SD; n = 3). Plants were grown for 10 days and seedlings cut 1 cm from the base were used for the analysis. The expression of mock-treated WT was set to 1 in each panel. n.s indicates no significant difference compared to WT or mock treated rice. (**K**) Lamina joint bending test of *smos* mutants. Addition of auxin and/or BL increase the lamina joint bending angle of WT, while *smos* mutants show attenuated bending compared to WT. PPBo; p-phenoxyphenyl boronic acid. One asterisk and two asterisks indicate statistically significant differences in comparison to the WT or mock treated rice ($P < 0.05$ and $P < 0.01$, respectively) (Dunnett, 1955).